

Theory of light scattering from a rough surface with an inhomogeneous dielectric permittivity

J. M. Elson

Research Department, Naval Weapons Center, China Lake, California 93555

(Received 28 November 1983; revised manuscript received 5 July 1984)

First-order perturbation theory is applied to calculate scattering of a plane wave from a plane-bounded, semi-infinite medium where the boundary surface has a roughness perturbation and the scattering medium consists of an isotropic perturbation of the dielectric permittivity. The dielectric perturbation is assumed to fluctuate randomly in the plane parallel to the surface and decay exponentially with depth into the surface. Both the roughness and dielectric permittivity perturbations, which are treated as random variables, can independently cause scattering, and there is generally interference between the two scattered fields. The scattered fields generally depend on the autocovariance functions of the surface roughness and dielectric fluctuations and on the cross-correlation properties between them. For this reason, the polarization ratio of the p - and s -polarized scattered light fields depends on the autocovariance and cross-correlation statistical properties. This result is unlike the calculation of scattered fields caused by roughness or dielectric perturbations alone, since in this case the polarization ratios of the scattered fields do *not* depend on the statistical properties of the perturbation. The numerical results of this work are consistent with experimental measurements where the polarization ratio of light scattered from nominally identical silver films varies widely from surface to surface.

I. INTRODUCTION

Encouraging agreement has been obtained between angular scattering from slightly rough optical surfaces predicted by a vector scattering theory and that measured directly.¹ The agreement has been particularly good for dielectric multilayers and for p -polarized scattering from opaque metal films. However, in many cases the measured s -polarized scattered light is considerably higher in the retroscattering direction than predicted.² Possible explanations are that the optical constants of the metal films are inhomogeneous in the vicinity of the surface, or that there is an additional thin surface film (tarnish) that is producing scattering anomalies. This paper addresses the question of inhomogeneous optical parameters (dielectric permittivity) which could represent inhomogeneities in the metal films, and shows that if these are assumed the polarization ratio in the scattered fields can be a variable dependent on surface statistical properties. This result is not possible if roughness-induced scattering is the only effect considered. The effect of scattering produced by thin tarnish films will also be discussed.

The experimental measurements which prompted the theoretical consideration of inhomogeneous optical constants have been briefly discussed in one published paper, and in two unpublished presentations.² Further experimental data will be presented here. Figure 1, reproduced from the published paper,² shows a typical measurement of angle-resolved scattering (ARS) from a polished, silver-coated, dense flint sample. The substrate surface roughness is uniform and isotropic, and scattering is measured in the plane of incidence at the retroscattering angle for an angle of incidence of 60° as shown in Fig. 2. The high-purity silver film, ~ 1000 Å thick, was evaporated in a vacuum of approximately 10^{-7} Torr. Other experimen-

tal details are not available, although this figure illustrates a typical result that has been observed in this laboratory and elsewhere³ for both evaporated and sputtered films deposited under a variety of conditions. In Fig. 1 the solid and dashed theoretical curves are calculated for ARS resulting from surface roughness. The surfaces are plane-bounded, slightly rough, semi-infinite surfaces where the scattering medium has a homogeneous and isotropic scalar dielectric constant (see Sec. II). In the calculations, the roughness of the film, measured using a Talys-

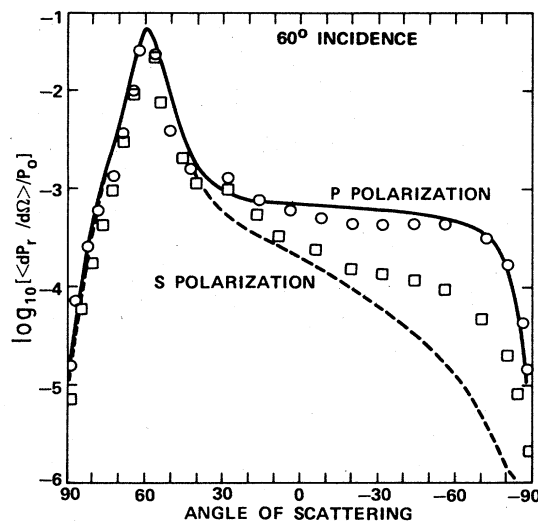


FIG. 1. Experimental (circles and squares) and predicted (solid and dashed curves) of angular scattering from a Ag-coated, dense flint sample for p - and s -polarized incident and scattered light, 60° angle of incidence, and $\lambda = 0.6328 \mu\text{m}$. The predicted curves are for roughness-only scattering in the plane of incidence.

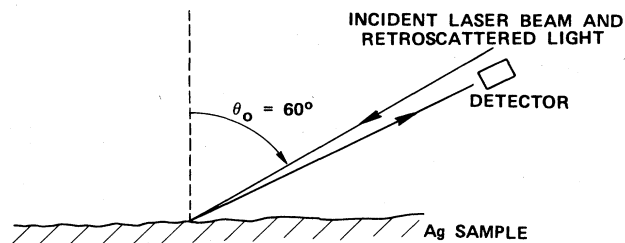


FIG. 2. Schematic diagram of retroscattering polarization ratio measurements for 60° incidence and $\lambda = 0.6328 \mu\text{m}$. The data in Table I were measured in this configuration.

tep surface-profiling instrument,⁴ has been slightly adjusted to make the theoretical curve for p polarization agree with the measured data (circles). No further adjustments can be made, i.e., the theoretical curve for s polarization is then fixed.

The deviation between theory and experiment for s -polarized scattered light increases as the backscattering angle increases, becoming a maximum for 90° backscattering. Different silver films have ARS curves of approximately the same shapes, with most of the variation occurring in the shape of the backscattering curve for s polarization. For this reason we have chosen to use as an indication of agreement between theory and experiment the retroscattering ratio $(p \rightarrow p)/(s \rightarrow s)$ for 60° incidence. (The agreement between theory and experiment is better for smaller angles of incidence.¹) As will be shown in Sec. II, this ratio is independent of the surface roughness if roughness-only scattering theory is used. In addition, all first-order scattering theories predict no cross-polarized scattered light in the plane of incidence, i.e., no p -(s -) polarized incident and s -(p -) polarized scattered light.

Table I lists experimental measurements of the $(p \rightarrow p)/(s \rightarrow s)$ retroscattering ratio for several silver films deposited onto commercially polished, fused-quartz substrates. Some of the films were subsequently baked in vacuum for 2 h at the temperatures indicated in the table. Cross-polarized scattering ratios $(s \rightarrow p)/(s \rightarrow s)$ were also measured. These results are typical of measurements

made at Michelson Laboratory on over 30 evaporated and sputtered silver films. A variety of cleaning procedures were tried, as were different roughness substrates, but there was relatively little effect on the results. In all cases the polarization ratio was measured within a few hours or at most a few days after the silver films had been deposited. (When there was going to be a delay before the retroscattering measurement could be made, the samples were stored in a nitrogen-filled dry box.) As shown in Table I, the polarization ratios are quite low, generally under 10, and vary from sample to sample; variations were also noted from place to place on a given sample. When a noticeable roughening of the film was produced by baking, the magnitude of both s - and p -polarized scattered light increase and the polarization ratio for retroscattered light also increased. The increase in roughening was shown, by electron microscopy, to be directly correlated with the growth of silver grains in the film.²

At the start of the study, retroscattering ratios were measured on silver- and aluminum-coated samples as well as on polished and diamond-turned copper samples. Some of these samples had remained in laboratory air for as long as several months, and were presumably covered with tarnish films. Silver sulfide tarnish films grow slowly as an open-pored structure, and do not reach a maximum thickness as long as there is silver remaining.⁵ Aluminum oxide, on the other hand, grows as a closed-pore film until it reaches a maximum thickness of 25–30 Å. Both silver- and aluminum-coated, tarnished samples exhibited anomalies in the retroscattering ratios—large variations (3 to 80) from sample to sample,² as well as variations from point to point on an individual sample. Additionally, some rougher silver-coated substrates containing large scratches and other macrodefects had quite large polarization ratios.² These large values could have been caused by the macrodefects or by surface films. In the initial measurements, there may also have been small experimental uncertainties caused by optical misalignment, orientation of the polarizer, analyzer, or half-wave plate, etc. Typically the retroscattering measurements were good to about 10%. Before each measurement was

TABLE I. Measured polarization ratios for evaporated and sputtered silver films that are subsequently baked in vacuum for 2 h at the temperatures indicated. The first five samples are sputtered silver films and the last five samples are evaporated silver films. The notations $p \rightarrow p$ and $s \rightarrow s$ refer to the polarization of the incident and scattered light, respectively, all measured relative to the plane of incidence. The angle of incidence was 60° , and 60° retroscattering was measured in the plane of incidence, all for a wavelength of 6328 Å.

Film No.	Temperature (°C)	rms roughness (Å)	$(p \rightarrow p)/(s \rightarrow s)$	$(s \rightarrow p)/(s \rightarrow s)$
17	Unbaked	4.2	3.9	0.2
19	50	6.3	3.3	0.2
3	100	3.8	1.3	0.2
16	200	5.1	3.5	0.25
11	250	10.3	13.7	0.3
3	Unbaked	5.9	10.4	0.25
4	50	4.5	3.6	0.3
36	100	6.6	9.1	0.3
5	200	11.0	3.2	0.1
9	250	7.8	19.7	0.4

made, the sample was translated until a low scatter spot was observed (laser-beam size was ~ 1 mm), to avoid effects of particulates and defects in the film or on the underlying substrate.

The question of what optical constants to use in the calculation of the retroscattering polarization ratio has also been considered. There was found to be almost no effect on the retroscattering polarization ratio even when calculations were made using the most widely differing published optical constants for silver. In fact, the difference between the retroscattering polarization ratios for silver, aluminum, and copper is also small: 39.7 for silver, 29.5 for aluminum, and 33.6 for copper at a wavelength of 6328 Å and a 60° angle of incidence. In the limit of a perfect conductor, $\epsilon \rightarrow \infty$, the ratio approaches 49. Since the 60° retroscattering polarization ratios were under 10 for all well-documented silver films except for baked (and roughened) ones, we can conclude that the choice of the average value of ϵ is not important.

Although no well-controlled experiments have been made on silver samples covered with known thicknesses of silver sulfide tarnish films, a few isolated measurements have been made. In one case, a retroscattering polarization ratio changed from about 35 (for a baked evaporated silver film) to 16 in a period of about three weeks.

In summary, the experimental data indicate the following. (1) There are large unexplained variations in the ($p \rightarrow p$)/($s \rightarrow s$) retroscattering polarization ratio for silver films (a) from sample to sample, and (b) for different places on the same sample. (2) All retroscattering ratios measured on freshly prepared evaporated or sputtered films are much lower than theoretically predicted values due to surface roughness alone, and (3) these ratios are too low to be explained by an incorrect choice of optical constants of silver. (4) The low ratios cannot be explained by surface-plasmon effects in silver because they also occur for aluminum films and diamond-turned and polished copper, neither of which have significant surface-plasmon resonances in the visible portion of the spectrum. (5) The presence of macrodefects on substrates are then contoured by the films probably affects the ratio; also, the presence of a thin, naturally occurring tarnish film can have an effect.

In this paper we will consider three different aspects of ARS perturbation theory: (1) ARS from slightly rough surface perturbations on semi-infinite surfaces where the scattering medium has a homogeneous, isotropic, scalar, and constant dielectric permittivity, (2) ARS from smooth, semi-infinite surfaces where the scattering medium consists of statistically isotropic but spatially variable scalar dielectric permittivity perturbations, and (3) ARS from plane-bounded media having both roughness and dielectric perturbations.

Since we are working in the framework of first-order perturbation theory, the calculations for cases (1) and (2) are independent and can be done separately. Thus, the final solution (3), which incorporates the effects of both roughness and dielectric fluctuations, is simply a linear superposition of both solutions. To give the reader pertinent background material and clarify the motivation for this calculation, we first discuss scattering from surface

roughness, as in case (1) above.

There have been numerous first-order calculations of light scattering from slightly rough, semi-infinite surfaces (excluding surfaces covered with multilayer dielectric films) where the vector properties of the scattering field are retained.^{6,7} These and other calculations have made use of various methods to arrive at a common result for the predicted ARS. For completeness, one such calculation will be outlined here and will be compared with scattering calculated from a theory taking into account dielectric permittivity fluctuations. The ARS formulas for scattering from slightly rough surfaces are proportional to the power spectral density of the surface roughness. Furthermore, these scattering formulas predict no cross-polarization ARS in the plane of incidence. In other words, for a p - (s -) polarized incident beam [electric vector parallel (perpendicular) to the plane of incidence], there will be only p - (s -) polarized scattered light in the plane of incidence. However, for directions out of the plane of incidence, there will generally be a mixture of s - and p -polarized scattered light (measured relative to the scattering plane). Although the formulas derived here are valid for arbitrary scattering directions and complex dielectric constants, the numerical results only consider scattering in the plane of incidence. Because there is no predicted cross polarization and the scattering should be proportional to the power spectral density of the surface roughness, it is straightforward to predict a polarization ratio of p - to s -polarized scattered light in the plane of incidence. This polarization ratio is determined from the theoretical expressions for p -polarized incident to p -polarized scattered and s -polarized incident to s -polarized scattered light. The theoretical polarization ratio should be independent of the statistical properties of the surface roughness (because the power-spectral-density function cancels out in the ratio) and dependent only on the dielectric properties of the material and angles of incidence and scattering. In other words, for given angles of incidence and scattering, the polarization ratio is predicted to be a constant for different samples of the same material. This theoretical ratio will be given explicitly in Sec. II. However, as discussed above, experimental values of the 60° retroscattering polarization ratio for opaque evaporated silver films are quite variable from one sample to another, and even at different places on the same sample.² Since these samples are of high quality, first-order scattering theory would be expected to apply. Thus we conclude that there may be an additional scattering mechanism other than surface roughness. The additional mechanism which is considered here is case (2) mentioned above, where the spatially variable dielectric permittivity is assumed to fluctuate randomly about a constant background value. This subject has been briefly discussed previously.^{2,8}

The paper is organized in the following manner. In Sec. II we outline the calculation of ARS from surface roughness. In Sec. III we describe the calculation of ARS from dielectric fluctuations. In Sec. IV we show the combined effect of roughness and dielectric fluctuations, while numerical results are given in Sec. V. Finally, in Sec. VI we summarize the results and give some conclusions.

II. SCATTERING FROM SURFACE ROUGHNESS

A. Boundary conditions

Here we calculate ARS from surface roughness for the case where the root-mean-square roughness ξ_r is much less than the incident wavelength λ . The rough surface is described by $z = \Delta z(x, y)$ and $\xi_r^2 = \langle [\Delta z(x, y)]^2 \rangle$, where $\langle \dots \rangle$ denotes an ensemble average. The mean surface is $z = 0$ since $\langle \Delta z(x, y) \rangle = 0$. The method of calculation, based on satisfying the boundary conditions to first order across the rough interface, has been called the equivalent-surface-current model.⁸ Physically, the rough surface is replaced by an equivalent plane sheet of surface currents which are proportional to the Dirac δ function and the surface height $\Delta z(x, y)$. As discussed by Jackson⁹ and Kröger and Kretschmann,⁸ the Dirac δ -function surface currents require discontinuities in the tangential components of the electric and magnetic fields across the surfaces. The method used here, matching boundary conditions, is now outlined.

As shown in Fig. 3, the rough interface between medium 1 and medium 2 has a unit vector normal given to first order by

$$\hat{n} = \hat{z} - \hat{x} \left[\frac{\partial \Delta z(x, y)}{\partial x} \right] - \hat{y} \left[\frac{\partial \Delta z(x, y)}{\partial y} \right], \quad (1)$$

where \hat{x} , \hat{y} , and \hat{z} are Cartesian unit vectors. In order to match boundary conditions at the surface, the electric field in medium 1 or 2 may be expanded about the $z = 0$ plane to approximate the electric field at $z = \Delta z(\vec{\rho})$; this is given by

$$\begin{aligned} \vec{E}_j(\vec{\rho}, \Delta z(\vec{\rho})) &= \vec{E}_j^{(0)}(\vec{\rho}, 0) + \Delta z(\vec{\rho}) \left[\frac{\partial}{\partial z} \vec{E}_j^{(0)}(\vec{\rho}, z) \right]_{z=0} \\ &+ \vec{E}_j^{(1)}(\vec{\rho}, 0), \end{aligned} \quad (2)$$

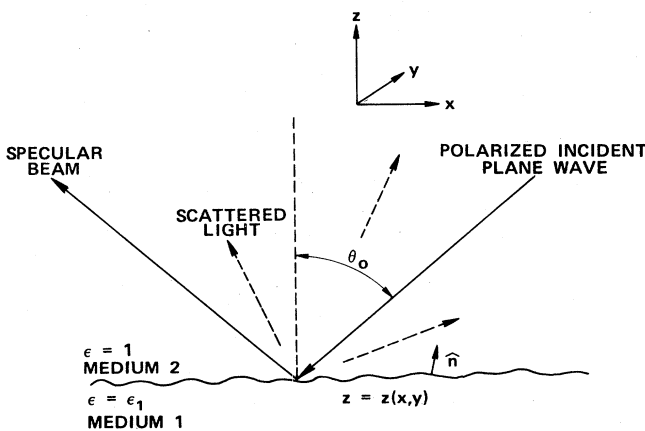


FIG. 3. Schematic diagram of nomenclature representing scattering from a plane-bounded, semi-infinite medium characterized by a homogeneous dielectric constant where the surface boundary is perturbed about the $z = 0$ plane according to $z = z(x, y)$. The plane wave is incident at an angle θ_0 measured from the normal.

where $\vec{\rho} = (x, y)$ and the medium is denoted by $j = 1$ or 2 (see Fig. 3). The $\vec{E}^{(0)}$ is the zeroth-order field, i.e., that field which could be calculated for a perfectly smooth surface for which $\Delta z(\vec{\rho}) = 0$. $\vec{E}^{(1)}$ is the first-order correction to the field which arises as a result of the rough interface. Consider first the boundary condition that the tangential components of the electric field given in Eq. (2) be continuous across the interface:

$$\hat{n} \times \Delta \vec{E}(\vec{\rho}, \Delta z(\vec{\rho})) = 0. \quad (3)$$

where

$$\Delta \vec{E}(\vec{\rho}, \Delta z(\vec{\rho})) = \vec{E}_2(\vec{\rho}, \Delta z(\vec{\rho})) - E_1(\vec{\rho}, \Delta z(\vec{\rho}))$$

is the difference of the electric fields evaluated across the $z = \Delta z(\vec{\rho})$ boundary. Using Eqs. (1) and (2) in Eq. (3) yields

$$\Delta E_x^{(1)} = - \left[\frac{\partial \Delta z(\vec{\rho})}{\partial x} \right] \Delta E_z^{(0)} - \Delta z(\vec{\rho}) \Delta \left[\frac{\partial E_x^{(0)}}{\partial x} \right] \quad (4a)$$

and

$$\Delta E_y^{(1)} = - \left[\frac{\partial \Delta z(\vec{\rho})}{\partial y} \right] \Delta E_z^{(0)} - \Delta z(\vec{\rho}) \Delta \left[\frac{\partial E_y^{(0)}}{\partial z} \right] \quad (4b)$$

for discontinuities of the x and y components of $\vec{E}^{(1)}$. The fields in Eqs. (4) have been evaluated at $z = 0$. Let the first- and zeroth-order fields have the form

$$\vec{E}^{(1)}(\vec{\rho}, z) = \int d^2 k \vec{e}^{(1)}(\vec{k}, z) e^{i \vec{k} \cdot \vec{\rho}} \quad (5a)$$

and

$$\vec{E}^{(0)}(\vec{\rho}, z) = \vec{e}^{(0)}(k_0, z) e^{i k_0 x}, \quad (5b)$$

respectively, whereby the field discontinuities at $z = 0$ are given by

$$\Delta \vec{E}^{(1)}(\vec{\rho}, 0) = \int d^2 k \Delta \vec{e}^{(1)}(\vec{k}, 0) e^{i \vec{k} \cdot \vec{\rho}} \quad (6a)$$

and

$$\Delta \vec{E}^{(0)}(\vec{\rho}, 0) = \Delta \vec{e}^{(0)}(k_0, 0) e^{i k_0 x}, \quad (6b)$$

respectively. An $\exp(-i\omega t)$ time dependence has been assumed, but it is not explicitly shown. Multiplying both sides of Eqs. (4) by $\exp(-i \vec{k}' \cdot \vec{\rho}) d^2 \rho$ and integrating yields

$$(2\pi)^2 \Delta e_x^{(1)}(\vec{k}) = -i k_x \Delta e_z^{(0)}(k_0, 0) \Delta z(\vec{k}_0 - \vec{k}) \quad (7a)$$

and

$$(2\pi)^2 \Delta e_y^{(1)}(\vec{k}) = -i k_y \Delta e_z^{(0)}(k_0, 0) \Delta z(\vec{k}_0 - \vec{k}), \quad (7b)$$

where

$$\Delta z(\vec{k}_0 - \vec{k}) = \int d^2 k \Delta z(\vec{\rho}) e^{i(\vec{k}_0 - \vec{k}) \cdot \vec{\rho}}. \quad (8)$$

Equation (8) is the Fourier transform of the interface profile. Similar equations hold for the tangential components of the magnetic field:

$$(2\pi)^2 \Delta h_x^{(1)}(\vec{k}) = i(\omega/c) \Delta z(\vec{k}_0 - \vec{k}) \Delta d_y^{(0)}(k_0, 0), \quad (9a)$$

$$(2\pi)^2 \Delta h_y^{(1)}(\vec{k}) = -i(\omega/c) \Delta z(\vec{k}_0 - \vec{k}) \Delta d_x^{(0)}(k_0, 0). \quad (9b)$$

The displacement vector $\vec{D}^{(0)}(\vec{\rho}, z) = \epsilon \vec{E}^{(0)}(\vec{\rho}, z)$, where $\epsilon = \epsilon_1$ for medium 1 and $\epsilon = 1$ for medium 2 (see Fig. 3). It follows that

$$\Delta \vec{D}^{(0)}(\vec{\rho}, 0) = \Delta \vec{d}^{(0)}(k_0, 0) \exp(ik_0 x)$$

is the difference of the zeroth-order displacement vector across the interface. To evaluate the right-hand sides of Eqs. (7) and (9), the zeroth-order fields are needed.

B. Zeroth-order field

The zeroth-order-field calculation is quite straightforward and only the results are presented here. Referring to Fig. 3, we consider the case of a plane wave incident at angle θ_0 relative to the z direction. In the incident and scattered fields, both p and s polarizations are considered. The zeroth-order solutions are written as

$$\vec{E}_2^{(0)}(\vec{\rho}, z) = \{[(\hat{x} \cos \theta_0 + \hat{z} \sin \theta_0) \cos \sigma + \hat{y} \sin \sigma] e^{-iq_0 z} + [R_p (\hat{x} \cos \theta_0 - \hat{z} \sin \theta_0) + \hat{y} R_s] e^{iq_0 z}\} e^{ik_0 x} \quad (10a)$$

and

$$\vec{E}_1^{(0)}(\vec{\rho}, z) = [(\hat{x} + \hat{z} k_0 / q) T_p + \hat{y} T_s] e^{i(k_0 x - yz)}, \quad (10b)$$

where

$$(1 + R_p) \cos \theta_0 = T_p, \quad (11a)$$

$$1 + R_s = T_s, \quad (11b)$$

and

$$R_p = \left[\frac{q - q_0 \epsilon_1}{q + q_0 \epsilon_1} \right] \cos \sigma, \quad (11c)$$

$$R_s = \left[\frac{q_0 - q}{q_0 + q} \right] \sin \sigma, \quad (11d)$$

$$T_p = \left[\frac{2q \cos \theta_0}{q + q_0 \epsilon_1} \right] \cos \sigma, \quad (11e)$$

$$T_s = \left[\frac{2(\omega/c) \cos \theta_0}{q + q_0} \right] \sin \sigma. \quad (11f)$$

The projection of the incident wave vector onto the (x, y) plane is $\vec{k}_0 = \hat{x} k_0$, where $k_0 = (\omega/c) \sin \theta_0$ and $\omega/c = 2\pi/\lambda$. The wave numbers are $q_0 = (\omega/c) \cos \theta_0$ and $q = [(\omega/c)^2 \epsilon_1 - k_0^2]^{1/2}$. The angle σ is the polarization angle measured relative to the plane of incidence defined by (\hat{x}, \hat{z}) . For $\sigma = 0(\pi/2)$, the incident wave is p (s) polarized. The R_p , R_s , T_p , and T_s are reflection and transmission amplitudes for p - and s -polarized incident waves, respectively. Referring to Eqs. (6b), (10), and (11), we see that

$$\Delta e_z^{(0)}(k_0, 0) = \frac{-(1 - \epsilon_1) k_0 T_p}{q} = \frac{-2k_0(1 - \epsilon_1) \cos \sigma \cos \theta_0}{q + q_0 \epsilon_1}, \quad (12a)$$

$$\Delta d_x^{(0)}(k_0, 0) = (1 - \epsilon_1) T_p = \frac{2q(1 - \epsilon_1) \cos \sigma \cos \theta_0}{q + q_0 \epsilon_1}, \quad (12b)$$

$$\Delta d_y^{(0)}(k_0, 0) = (1 - \epsilon_1) T_s = \frac{2(\omega/c)(1 - \epsilon_1) \sin \sigma \cos \theta_0}{q + q_0}. \quad (12c)$$

C. First-order fields

To use the boundary conditions given in Eqs. (7) and (9) along with Eqs. (12) we assume the following explicit forms for the first-order fields in media 1 and 2, respectively:

$$\vec{E}_{1r}^{(1)}(\vec{\rho}, z) = -\frac{i(1 - \epsilon_1)}{(2\pi)^2} \int d^2 k \Delta z (\vec{k}_0 - \vec{k}) [(\hat{k} q_1 + \hat{z} k) p_{1r} - (\hat{k} \times \hat{z})(\omega/c) s_{1r}] e^{i(\vec{k} \cdot \vec{\rho} - q_1 z)} \quad (13a)$$

and

$$\vec{E}_{2r}^{(1)}(\vec{\rho}, z) = -\frac{i(1 - \epsilon_1)}{(2\pi)^2} \int d^2 k \Delta z (\vec{k}_0 - \vec{k}) [(\hat{k} q_2 - \hat{z} k) p_{2r} - (\hat{k} \times \hat{z})(\omega/c) s_{2r}] e^{i(\vec{k} \cdot \vec{\rho} + q_2 z)}, \quad (13b)$$

where \hat{k} is a unit vector such that $\vec{k} = \hat{k} k$. The r subscript refers to roughness. Furthermore, the magnetic fields may be derived from Eqs. (13) by applying $\vec{\nabla} \times \vec{E} = -i(\omega/c) \vec{H}$ to yield

$$\vec{H}_{1r}^{(1)}(\vec{\rho}, z) = \frac{i(1 - \epsilon_1)}{(2\pi)^2} \int d^2 k \Delta z (\vec{k}_0 - \vec{k}) [(\hat{k} q_1 + \hat{z} k) s_{1r} + (\hat{k} \times \hat{z}) \epsilon_1 (\omega/c) p_{1r}] e^{i(\vec{k} \cdot \vec{\rho} - q_1 z)}, \quad (14a)$$

$$\vec{H}_{2r}^{(1)}(\vec{\rho}, z) = \frac{i(1 - \epsilon_1)}{(2\pi)^2} \int d^2 k \Delta z (\vec{k}_0 - \vec{k}) [(\hat{k} q_2 - \hat{z} k) s_{2r} + (\hat{k} \times \hat{z}) (\omega/c) p_{2r}] e^{i(\vec{k} \cdot \vec{\rho} - q_2 z)}. \quad (14b)$$

The components of the wave vector of the scattered light is given by $(\vec{k}, -q_1)$ for Eqs. (13a) and (14a), and (\vec{k}, q_2) for Eqs. (13b) and (14b), where

$$q_1 = [(\omega/c)^2 \epsilon_1 - k^2]^{1/2} \quad \text{and} \quad q_2 = [(\omega/c)^2 - k^2]^{1/2}.$$

The vector \vec{k} is the projection of the scattered-light wave vector onto the (\hat{x}, \hat{y}) plane where $\vec{k} = \hat{x}k_x + \hat{y}k_y$. Using Eqs. (13) and (14) in Eqs. (7) and (9) with Eqs. (12) yields the following solutions for the scattering coefficients p_{1r} , p_{2r} , s_{1r} , and s_{2r} :

$$p_{1r} = \frac{2 \cos \theta_0}{q_1 + q_2 \epsilon_1} \left[\frac{(q q_2 \cos \phi + k k_0) \cos \sigma}{q + q_0 \epsilon_1} + \frac{(\omega/c) q_2 \sin \phi \sin \sigma}{q + q_0} \right], \quad (15a)$$

$$p_{2r} = \frac{2 \cos \theta_0}{q_1 + q_2 \epsilon_1} \left[\frac{(q q_1 \cos \phi - k k_0 \epsilon_1) \cos \sigma}{q + q_0 \epsilon_1} + \frac{(\omega/c) q_1 \sin \phi \sin \sigma}{q + q_0} \right], \quad (15b)$$

$$s_{1r} = s_{2r} = \frac{2(\omega/c) \cos \theta_0}{q_1 + q_2} \left[\frac{(\omega/c) \cos \phi \sin \sigma}{q + q_0} - \frac{q \sin \phi \cos \sigma}{q + q_0 \epsilon_1} \right]. \quad (15c)$$

The p_{1r} and p_{2r} coefficients refer to p -polarized scattered light [light polarized parallel to the plane of scattering, which is defined by the (\vec{k}, \hat{z}) plane]. The s_{1r} and s_{2r} coefficients refer to s -polarized scattering light (light polarized perpendicular to the scattering plane). The angle ϕ is the azimuthal scattering angle such that $\vec{k} = k(\hat{x} \cos \phi + \hat{y} \sin \phi)$ and $\vec{k} = \hat{k}k$, where $\hat{k} = \hat{x} \cos \phi + \hat{y} \sin \phi$. Again, the angle σ refers to the polarization of the incident beam. Equations (15a)–(15c) may be written in terms of Eqs. (11e) and (11f) as

$$p_{1r} = \frac{1}{q_1 + q_2 \epsilon_1} \left[q_2 (T_p \cos \phi + T_s \sin \phi) + \frac{k k_0 T_p}{q} \right], \quad (15d)$$

$$p_{2r} = \frac{1}{q_1 + q_2 \epsilon_1} \left[q_1 (T_p \cos \phi + T_s \sin \phi) - \frac{k k_0 \epsilon_1 T_p}{q} \right], \quad (15e)$$

$$s_{1r} = s_{2r} = \frac{\omega/c}{q_1 + q_2} (T_s \cos \phi - T_p \sin \phi). \quad (15f)$$

This form of p_{1r} , p_{2r} , s_{1r} , and s_{2r} will be easier to compare directly to the corresponding terms for scattering from dielectric fluctuations.

D. Angle-resolved scattering

To obtain the expression for the ARS into medium 2, consider the time-averaged Poynting vector of the first-order fields,

$$\vec{S}_2^{(1)} = \frac{c}{8\pi} \text{Re}(\vec{E}_2^{(1)} \times \vec{H}_2^{(1)*}), \quad (16)$$

where the $*$ denotes complex conjugate. To obtain the

first-order power radiated away from the surface, we calculate

$$P_r = \int d^2 \rho \vec{S}_2^{(1)} \cdot \hat{z}, \quad (17a)$$

where the integration is over the surface and the subscript r refers to roughness scattering. This yields

$$P_r = \frac{\omega |1 - \epsilon_1|^2}{4(2\pi)^3} \int d^2 k q_2 |\Delta z(\vec{k}_0 - \vec{k})|^2 \times [|p_{2r}|^2 + |s_{2r}|^2] e^{-2z \text{Im}(q_2)}. \quad (17b)$$

Note that

$$q_2 = [(\omega/c)^2 - k^2]^{1/2}.$$

If $k \leq \omega/c$, the exponential term of Eq. (17b) is unity, but if $k > \omega/c$, the exponential term does not allow energy to radiate into medium 2. Thus, as far as scattered light is concerned, we are only interested in situations where $k = (\omega/c) \sin \theta < \omega/c$, with θ being the polar scattering angle measured relative to the z direction. Since $k_x = k \cos \phi$ and $k_y = k \sin \phi$, it is straightforward to show that

$$d^2 k = (\omega/c)^2 \cos \theta d\Omega,$$

where $d\Omega = \sin \theta d\theta d\phi$. In addition, the total power incident on the surface may be shown from Eq. (10a) to be $P_0 = (c/8\pi) L^2 \cos \theta_0$, where L^2 is the area of the illuminated beam. Thus, Eq. (17b) may be written in differential form and normalized with respect to the incident power as

$$\frac{1}{P_0} \frac{dP_r}{d\Omega} = \frac{(\omega/c)^4 |1 - \epsilon_1|^2 \cos^2 \theta}{(2\pi)^2 \cos \theta_0} [|p_{2r}|^2 + |s_{2r}|^2] \times \frac{|\Delta z(\vec{k}_0 - \vec{k})|^2}{L^2}. \quad (18a)$$

This equation represents the fraction of the incident power scattered into direction (θ, ϕ) per unit solid angle $d\Omega$. The power spectral density of the surface roughness is given by $|\Delta z(\vec{k}_0 - \vec{k})|^2 / L^2$. In this paper only random, nondeterministic surfaces are considered. Thus, Eq. (18a) needs to be ensemble-averaged to provide an average fractional scattered power. The ensemble average acts only on $|\Delta z(\vec{k}_0 - \vec{k})|^2 / L^2$, yielding

$$\frac{1}{P_0} \left\langle \frac{dP_r}{d\Omega} \right\rangle = \frac{(\omega/c)^4 |1 - \epsilon_1|^2 \cos^2 \theta}{(2\pi)^2 \cos \theta_0} [|p_{2r}|^2 + |s_{2r}|^2] \times g_r(\vec{k}_0 - \vec{k}), \quad (18b)$$

where the average power spectral density of the surface roughness is denoted by

$$g_r(\vec{k}_0 - \vec{k}) = \frac{\langle |\Delta z(\vec{k}_0 - \vec{k})|^2 \rangle}{L^2}. \quad (19a)$$

The area L^2 is assumed to approach infinity. The term $g_r(\vec{k}_0 - \vec{k})$ is the two-dimensional Fourier transform of the autocovariance function of the surface roughness

$$G_r(\vec{\tau}) = \langle \Delta z(\vec{\rho}) \Delta z(\vec{\rho} + \vec{\tau}) \rangle,$$

or

$$g_r(\vec{K}) = \int d^2\tau G_r(\vec{\tau}) e^{i\vec{K} \cdot \vec{\tau}}, \quad (19b)$$

where $G(0) = \xi_r^2$ is the mean-square roughness and has dimensions of length squared.

Equations (18) are proportional to $(\omega/c)^4$ or λ^{-4} . This is characteristic of Rayleigh scattering. Physically, this occurs in the perturbation calculation because the Born approximation is used, which is valid when the ratio $\xi_r/\lambda \ll 1$. In other words, the average vertical deviation from the $z=0$ plane is much smaller than the wavelength of illuminating light. Rayleigh scattering occurs when the roughness height is much smaller than λ and the shape of the scatterer is unimportant. The parameter ξ_r is influential in the amplitude of the scattered fields. However, the angular distribution of power scattered from the surface requires a knowledge of the lateral properties of the surface roughness. This information is implicit in $g_r(\vec{K})$ and $G_r(\vec{\tau})$ and appears only in the ARS formula. Note that the fractional scattered power in Eq. (18b) is proportional to the power spectral density of the roughness $g_r(\vec{k}_0 - \vec{k})$ and the square of the dielectric mismatch $|1 - \epsilon_1|^2$.

E. Polarization ratio

As mentioned in Sec. I, the expected polarization ratio for the scattered light may be calculated from Eq. (18b). Considering only the plane of incidence, we set $\phi=0$ or π depending on whether the scattering is the forward quadrant (quadrant containing the specular beam) or backward quadrant (quadrant containing the incident beam). For normal incidence, this distinction does not apply. Consider first $\sigma=0$, or p -polarized incident light. For scattering into medium 2, we have, from Eq. (15b),

$$p_{2r} = \frac{2 \cos\theta_0 (qq_1 \cos\phi - kk_0 \epsilon_1)}{(q_1 + q_2 \epsilon_1)(q + q_0 \epsilon_1)}, \quad (20a)$$

where $\cos\phi = \pm 1$, as discussed above. The s_{2r} coefficient vanishes, indicating that only p -polarized scattered light is predicted for p -polarized incident light. Letting $\sigma = \pi/2$ for s -polarized incident light yields $p_{2r} = 0$, and

$$s_{2r} = \frac{2(\omega/c)^2 \cos\theta_0 \cos\phi}{(q_1 + q_2)(q + q_0)}. \quad (20b)$$

Using Eqs. (20) in Eq. (18b) yields the differential scattered power for each incident polarization. Thus, we may calculate the ratio ξ_r of p -polarized to s -polarized scattered power, which yields

$$\begin{aligned} \xi_r &= \left\langle \frac{dP_r^p}{dP_r^s} \right\rangle = |p_{2r}/s_{2r}|^2 \\ &= \frac{|(q_1 + q_2)(q + q_0)(qq_1 \cos\phi - kk_0 \epsilon_1)|^2}{(\omega/c)^4 |(q_1 + q_2 \epsilon_1)(q + q_0 \epsilon_1)|^2}. \end{aligned} \quad (21)$$

Note that the ratio in Eq. (21) does not depend on the surface-roughness statistics, which are embodied in

$g_r(\vec{k}_0 - \vec{k})$, since this quantity cancels out. The ratio does depend on parameters such as the angle of incidence θ_0 , the angles of scattering (θ, ϕ) , wavelength, and dielectric constant ϵ_1 . The interesting prediction of this result is that for roughness scattering from surfaces which have $\xi_r \ll \lambda$, the polarization ratio should be a constant for samples of different roughness. However, as discussed in Sec. I, this is contrary to experimental observations. The experimentally measured polarization ratio is only close to the value predicted by roughness scattering theory for a few silver films which have been baked in vacuum and considerably roughened.

III. SCATTERING FROM DIELECTRIC FLUCTUATIONS

A. Wave equation

Computationally and physically, this calculation is significantly different from that of Sec. II. Physically, the polarization scattering currents are located in the bulk rather than on the surface of the material. Surface roughness is not considered in this section. Referring to Fig. 4, we see that the medium from which the scattering occurs (medium 1, $z \leq 0$) is assumed to consist of a scalar dielectric permittivity of the form

$$\epsilon(\vec{\rho}, z) = \epsilon_1 + \Delta\epsilon(\vec{\rho}, z), \quad (22a)$$

where ϵ_1 is a constant independent of position, and $\Delta\epsilon$ is a random variable which fluctuates around the background value ϵ_1 . By analogy to the random fluctuations of $\Delta z(\vec{\rho})$ for the surface-roughness calculation, we assume $\langle \Delta\epsilon(\vec{\rho}, z) \rangle = 0$. To further simplify matters, we further assume an analytical z dependence where

$$\Delta\epsilon(\vec{\rho}, z) = \Delta\epsilon(\vec{\rho}) e^{\alpha z}, \quad z \leq 0. \quad (22b)$$

Thus, the random part of $\epsilon(\vec{\rho}, z)$ depends only on $\vec{\rho}$, and the z dependence is exponential with a decay constant α . With these assumptions, the dielectric fluctuations may be thought of as columnar in nature since there is no statisti-

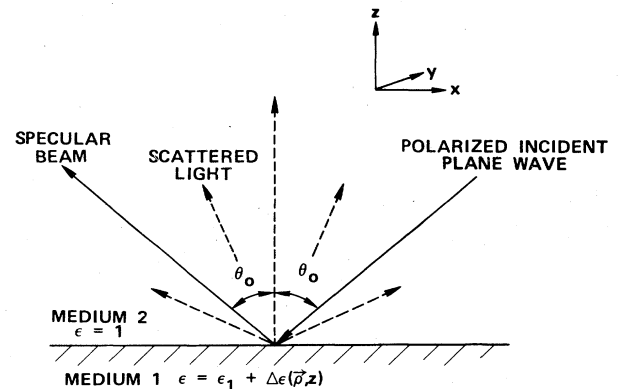


FIG. 4. Schematic diagram of nomenclature concerning scattering from a smooth, plane-bounded semi-infinite medium characterized by an inhomogeneous dielectric permittivity $\epsilon(\vec{\rho}, z)$. The plane wave is incident at an angle θ_0 measured from the normal.

cal variation in the z direction. The parameter α controls the effective depth of the columnar structure and, consequently, of the scattering volume. The mean-square value of the magnitude of $\Delta\epsilon(\vec{\rho})$ is

$$\langle |\Delta\epsilon(\vec{\rho})|^2 \rangle = \zeta_d^2. \quad (23)$$

Considering Maxwell's equations,

$$\vec{\nabla} \times \vec{H} = -i(\omega/c)\epsilon\vec{E}, \quad (24a)$$

$$\vec{\nabla} \times \vec{E} = i(\omega/c)\vec{H}, \quad (24b)$$

the wave equation may be written in the following two forms:

$$\vec{\nabla} \times \vec{\nabla} \times \vec{E} - (\omega/c)^2\epsilon\vec{E} = 0 \quad (25a)$$

or

$$\nabla^2\vec{E} + (\omega/c)^2\epsilon\vec{E} = \vec{\nabla}(\vec{\nabla} \cdot \vec{E}). \quad (25b)$$

In the case of a homogeneous dielectric medium, the $\vec{\nabla} \cdot \vec{E}$ term is typically set equal to zero and Eq. (25b) is often used as a starting point. However, in this paper $\vec{\nabla} \cdot \vec{E} \neq 0$ in medium 1; to avoid having to initially specify the detailed form of $\vec{\nabla} \cdot \vec{E}$, Eq. (25a) is taken as the starting point. Using the ϵ given in Eq. (22a) in Eq. (25a), the fields $\vec{E}_1(\vec{\rho}, z)$ and $\vec{E}_2(\vec{\rho}, z)$ satisfy the equations

$$\begin{aligned} \vec{\nabla} \times \vec{\nabla} \times \vec{E}_1(\vec{\rho}, z) - (\omega/c)^2\epsilon_1\vec{E}_1(\vec{\rho}, z) \\ = (\omega/c)^2\Delta\epsilon(\vec{\rho})e^{i\alpha z}\vec{E}_1(\vec{\rho}, z) \end{aligned} \quad (26a)$$

and

$$\vec{\nabla} \times \vec{\nabla} \times \vec{E}_2(\vec{\rho}, z) - (\omega/c)^2\vec{E}_2(\vec{\rho}, z) = 0 \quad (26b)$$

for regions 1 and 2, respectively. In Eqs. (26) the field \vec{E}_1 is generated by the source term on the right-hand side of Eq. (26a) and the field E_2 is also generated by the same source term, except that \vec{E}_2 is in a source-free region.

B. First-order fields

The solutions to Eqs. (26) are obtained by a Green's-function approach where

$$\underline{L} = \begin{pmatrix} -\frac{\partial^2}{\partial y^2} - \frac{\partial^2}{\partial z^2} - (\omega/c)^2\epsilon_1 & \frac{\partial^2}{\partial y \partial x} & \frac{\partial^2}{\partial z \partial x} \\ \frac{\partial^2}{\partial x \partial y} & -\frac{\partial^2}{\partial x^2} - \frac{\partial^2}{\partial z^2} - (\omega/c)^2\epsilon_1 & \frac{\partial^2}{\partial y \partial z} \\ \frac{\partial^2}{\partial x \partial z} & \frac{\partial^2}{\partial y \partial z} & -\frac{\partial^2}{\partial y^2} - \frac{\partial^2}{\partial x^2} - (\omega/c)^2\epsilon_1 \end{pmatrix}. \quad (29)$$

To solve Eq. (28) we need to calculate the 3×3 Green's matrix $\underline{G}(\vec{r}, \vec{r}')$, which satisfies the relation

$$\underline{L} \underline{G}(\vec{r}, \vec{r}') = \underline{I} \delta^3(\vec{r} - \vec{r}'), \quad (30)$$

where \underline{I} is the 3×3 identity matrix. The vectors \vec{r} and \vec{r}' are the observation and source locations, respectively. If we further let

$$\underline{G}(\vec{r}, \vec{r}') = \left[\frac{1}{2\pi} \right]^2 \int d^2k \underline{g}(z, z') e^{i\vec{k} \cdot (\vec{\rho} - \vec{\rho}')} \quad (31a)$$

$$\vec{E}(\vec{\rho}, z) = (\omega/c)^2 \int d^2\rho' dz' \Delta\epsilon(\vec{\rho}', z') \underline{G}(\vec{r}, \vec{r}') \vec{E}_1(\vec{\rho}', z'), \quad (27a)$$

and the integration is over the volume of medium 1. The question of whether $\vec{E}(\vec{\rho}, z)$ is $\vec{E}_1(\vec{\rho}, z)$ or $\vec{E}_2(\vec{\rho}, z)$ depends on the Green's-function matrix $\underline{G}(\vec{r}, \vec{r}')$. This will be discussed in more detail below.

At this point no size limits on the ratio $\zeta_d/|\epsilon_1|$ have been set since there is no analogy to the Born-approximation calculation. As shown below, a perturbation method will be used to obtain a closed-form solution, which means that the effect of $\Delta\epsilon(\vec{\rho})$ on the zero-order field must be small. From Eq. (26a) it follows that the perturbation method requires the magnitude of the source term, which is proportional to $\Delta\epsilon(\vec{\rho})$, to be small compared to the ϵ_1 term. It follows that $\zeta_d/|\epsilon_1| \ll 1$ will satisfy these requirements.

Equation (27a) is an integral equation and as such it is not easy to solve analytically. However, as discussed above, an analytical solution is straightforward when a perturbation expansion $\vec{E} = \vec{E}^{(0)} + \vec{E}^{(1)}$ is assumed where $\vec{E}^{(0)}$ and $\vec{E}^{(1)}$ are the zeroth- and first-order solutions, respectively. From Eq. (27a), we have

$$\vec{E}^{(1)}(\vec{\rho}, z) = (\omega/c)^2 \int d^2\rho' dz' \Delta\epsilon(\vec{\rho}', z') \underline{G}(\vec{r}, \vec{r}') \vec{E}_1^{(0)}(\vec{\rho}', z'), \quad (27b)$$

and since all quantities on the right-hand side can be calculated, the solutions to Eq. (27b), $\vec{E}_1^{(1)}(\vec{\rho}, z)$ and $\vec{E}_2^{(1)}(\vec{\rho}, z)$, can be obtained. To obtain these solutions the following approach is used.

Following Maradudin and Mills,¹⁰ we write the operator $\vec{\nabla} \times \vec{\nabla} \times \vec{E}$ in matrix form so that Eq. (26a) may be written

$$\underline{L} \vec{E}^{(1)} = (\omega/c)^2 \Delta\epsilon(\vec{\rho}) e^{i\alpha z} \vec{E}^{(0)}, \quad (28)$$

where $\vec{E}^{(1)}$ and $\vec{E}^{(0)}$ are three-component column vectors, and \underline{L} is a matrix operator written as

and

$$\delta^3(\vec{r}-\vec{r}')=\delta(z-z')\left[\frac{1}{2\pi}\right]^2\int d^2k e^{i\vec{k}\cdot(\vec{\rho}-\vec{\rho}')} , \quad (31b)$$

Eq. (30) may be solved for $\underline{G}(\vec{r},\vec{r}')$. The solutions have been published elsewhere.¹¹ However, for completeness, they are reproduced in Appendix A. As mentioned above, the particular solutions to Eqs. (26) are given in two parts. These include scattering from the dielectric fluctuations into mediums 1 and 2. With Eq. (31a) in Eq. (27b), these two solutions may be written as

$$\vec{E}_{1d}^{(1)}(\vec{\rho},z)=\left[\frac{\omega}{2\pi c}\right]^2\int d^2k d^2\rho' dz' \underline{g}^{(1,1)}(z,z')\vec{E}_1^{(0)}(\vec{\rho}',z')\Delta\epsilon(\vec{\rho}',z')e^{i\vec{k}\cdot(\vec{\rho}-\vec{\rho}')} \quad (32a)$$

and

$$\vec{E}_{2d}^{(1)}(\vec{\rho},z)=\left[\frac{\omega}{2\pi c}\right]^2\int d^2k d^2\rho' dz' \underline{g}^{(2,1)}(z,z')\vec{E}_1^{(0)}(\vec{\rho}',z')\Delta\epsilon(\vec{\rho}',z')e^{i\vec{k}\cdot(\vec{\rho}-\vec{\rho}')} , \quad (32b)$$

where the d subscript refers to dielectric fluctuation. If we let

$$\Delta\epsilon(\vec{k}_0-\vec{k})=\int d^2\rho' \Delta\epsilon(\vec{\rho}')e^{i(\vec{k}_0-\vec{k})\cdot\vec{\rho}'} , \quad (33)$$

and assume zeroth-order fields as in Eq. (5b), Eqs. (32) may be simplified to

$$\vec{E}_{1d}^{(1)}(\vec{\rho},z)=\left[\frac{\omega}{2\pi c}\right]^2\int d^2k dz' \underline{g}^{(1,1)}(z,z')\vec{e}_1^{(0)}(k_0,z')\Delta\epsilon(\vec{k}_0-\vec{k})e^{az'}e^{i\vec{k}\cdot\vec{\rho}} \quad (34a)$$

and

$$\vec{E}_{2d}^{(1)}(\vec{\rho},z)=\left[\frac{\omega}{2\pi c}\right]^2\int d^2k dz' \underline{g}^{(2,1)}(z,z')\vec{e}_1^{(0)}(k_0,z')\Delta\epsilon(\vec{k}_0-\vec{k})e^{az'}e^{i\vec{k}\cdot\vec{\rho}} . \quad (34b)$$

With the aid of the Green's functions as given in Appendix A, the dz' integration may be performed. Equation (32a) yields

$$\vec{E}_{1d}^{(1)}(\vec{\rho},z)=\left[\frac{1}{2\pi}\right]^2\frac{1}{\epsilon_1}\int d^2k \frac{\Delta\epsilon(\vec{k}_0-\vec{k})}{[q_1^2-(q+i\alpha)^2]}\{[\vec{A}_p(\vec{k})+\vec{A}_s(\vec{k})]e^{-iq_1z}-[\vec{B}_p(\vec{k})+\vec{B}_s(\vec{k})]e^{-i(q+i\alpha)z}\}e^{i\vec{k}\cdot\vec{\rho}} , \quad (35a)$$

where

$$\vec{A}_p(\vec{k},\alpha)=\frac{(\hat{k}q_1+\hat{z}k)}{q_2\epsilon_1+q_1}\left\{[(q+i\alpha)q_2\epsilon_1+q_1^2](T_p\cos\phi+T_s\sin\phi)+\frac{kk_0T_p(q+q_2\epsilon_1+i\alpha)}{q}\right\} , \quad (35b)$$

$$\vec{B}_p(\vec{k},\alpha)=[\hat{k}q_1^2+\hat{z}k(q+i\alpha)](T_p\cos\phi+T_s\sin\phi)+\frac{kk_0T_p}{q}[\hat{k}(q+i\alpha)+\hat{z}k] , \quad (35c)$$

$$\vec{A}_s(\vec{k},\alpha)=\frac{\hat{k}\times\hat{z}}{q_1+q_2}[(\omega/c)^2\epsilon_1(q+q_2+i\alpha)(T_p\sin\phi-T_s\cos\phi)] , \quad (35d)$$

and

$$\vec{B}_s(\vec{k})=(\hat{k}\times\hat{z})(\omega/c)^2\epsilon_1(T_p\sin\phi-T_s\cos\phi) . \quad (35e)$$

For the upper medium, Eq. (32b) yields

$$\vec{E}_{2d}^{(1)}(\vec{\rho},z)=-\left[\frac{1}{2\pi}\right]^2\int d^2k \frac{\Delta\epsilon(\vec{k}_0-\vec{k})}{q+q_1+i\alpha}[(\hat{k}q_2-\hat{z}k)p_{2d}-(\hat{k}\times\hat{z})(\omega/c)s_{2d}]e^{i\vec{k}\cdot\vec{\rho}+q_2z} , \quad (36a)$$

where

$$p_{2d}=\frac{1}{q_2\epsilon_1+q_1}[q_1(T_p\cos\phi+T_s\sin\phi)-kk_0T_p/q] \quad (36b)$$

and

$$s_{2d}=\frac{\omega/c}{q_1+q_2}(T_s\cos\phi-T_p\sin\phi) . \quad (36c)$$

The expressions for T_p and T_s are given by Eqs. (11e) and (11f). The magnetic field in medium 2 is given by

$$\vec{H}_{2d}^{(1)}(\vec{\rho}, z) = \left[\frac{1}{2\pi} \right]^2 \int d^2k \frac{\Delta\epsilon(\vec{k}_0 - \vec{k})}{q + q_1 + i\alpha} [(\hat{k}q_2 - \hat{z}k)s_{2d} + (\hat{k} \times \hat{z})(\omega/c)p_{2d}] e^{i(\vec{k} \cdot \vec{\rho} + q_2 z)}. \quad (36d)$$

Note that the scattered field in medium 2 [Eqs. (36)] is proportional to $(q + q_1 + i\alpha)^{-1}$. This term is related to the effective depth of the scattering volume with regard to α and the skin depth of the zeroth- and first-order fields. The units of $\Delta\epsilon(\vec{k}_0 - \vec{k})/(q + q_1 + i\alpha)$ are identical to $\Delta z(\vec{k}_0 - \vec{k})$. In the limit as $\alpha \rightarrow \infty$, the first-order fields $\vec{E}_{1d}^{(1)}$ and $\vec{E}_{2d}^{(1)}$ both approach zero as $1/\alpha$. This result is expected since the volume of dielectric fluctuations vanishes in this limit. In addition, the background dielectric constant ϵ_1 may be unity. In this case, the scattering medium may be thought of as air with density fluctuations. Letting $\epsilon_1 \rightarrow 1$ in the surface-roughness calculation causes the fields to vanish, whereas this does not happen for the dielectric fluctuation calculation.

In the special case where $\alpha = 0$ in Eqs. (35) and (36), the particular solution for the first-order field in medium 1 reduces to

$$\vec{E}_{1d}^{(1)}(\vec{\rho}, z) = \left[\frac{1}{2\pi} \right]^2 \frac{1}{\epsilon_1} \int d^2k \frac{\Delta\epsilon(\vec{k}_0 - \vec{k})}{k_0^2 - k^2} \{ [\vec{A}_p(\vec{k}, 0) + \vec{A}_s(\vec{k}, 0)] e^{-iq_1 z} - [\vec{B}_p(\vec{k}, 0) + \vec{B}_s(\vec{k})] e^{-iqz} \} e^{i\vec{k} \cdot \vec{\rho}}, \quad (37a)$$

where

$$\vec{A}_p(\vec{k}, 0) = \frac{\hat{k}q_1 + \hat{z}k}{q_2\epsilon_1 + q_1} \left[(q_1^2 + qq_2\epsilon_1)(T_p \cos\phi + T_s \sin\phi) + \frac{kk_0 T_p (q + q_2 \epsilon_1)}{q} \right], \quad (37b)$$

$$\vec{B}_p(\vec{k}, 0) = (\hat{k}q_1^2 + \hat{z}kq)(T_p \cos\phi + T_s \sin\phi) + \frac{k_0 T_p}{q} (\hat{k}kq + \hat{z}k_0^2), \quad (37c)$$

$$\vec{A}_s(\vec{k}, 0) = \frac{\hat{k} \times \hat{z}}{q_1 + q_2} [(\omega/c)^2 \epsilon_1 (q + q_2)(T_p \sin\phi - T_s \cos\phi)], \quad (37d)$$

and $\vec{B}_s(\vec{k})$ is unchanged since it does not depend on α . The corresponding solution for medium 2 is

$$\vec{E}_{2d}^{(1)}(\vec{\rho}, z) = - \left[\frac{1}{2\pi} \right]^2 \int d^2k \frac{\Delta\epsilon(\vec{k}_0 - \vec{k})}{q + q_1} [(\hat{k}q_2 - \hat{z}k)p_{2d} - (\hat{k} \times \hat{z})(\omega/c)s_{2d}] e^{i(\vec{k} \cdot \vec{\rho} + q_2 z)}. \quad (38)$$

In Eq. (37a) there appears to be a singularity at $k = k_0$. However, a careful comparison of Eqs. (37b)–(37d) with Eq. (35e) reveals that

$$\lim_{k \rightarrow k_0} [\vec{A}_p(\vec{k}, 0) e^{-iq_1 z} - \vec{B}_p(\vec{k}, 0) e^{-iqz}] = 0 \quad (39a)$$

and

$$\lim_{k \rightarrow k_0} [\vec{A}_s(\vec{k}, 0) e^{-iq_1 z} - \vec{B}_s(k) e^{-iqz}] = 0. \quad (39b)$$

Thus, it may be shown that the integral in Eq. (37a) is well behaved as $k \rightarrow k_0$.

The case where $\alpha = 0$ may be of interest for dielectric fluctuations which are not damped with distance into medium 1. This situation may occur for surfaces exhibiting infinite columnar structure.

Since Eqs. (35) and (36) are the particular solutions to the inhomogeneous dielectric scattering problem, we may investigate them directly to see that the proper divergence conditions are satisfied. We see from Eq. (36a) that $\vec{\nabla} \cdot \vec{E}_{2d}^{(1)}(\vec{\rho}, z) = 0$. From Eqs. (35) the divergence may be shown to be

$$\vec{\nabla} \cdot \vec{E}_{1d}^{(1)}(\vec{\rho}, z) = - \frac{i}{\epsilon_1} \left[\frac{1}{2\pi} \right]^2 \int d^2k \Delta\epsilon(\vec{k}_0 - \vec{k}) \left[k(T_p \cos\phi + T_s \sin\phi) - \frac{k_0 T_p}{q} (q + i\alpha) \right] e^{i[\vec{k} \cdot \vec{\rho} - (q + i\alpha)z]}. \quad (40)$$

To check the accuracy of these divergence expressions, we consider the induced polarization charge density, as discussed in the next section.

C. Induced polarization charge density in the inhomogeneous medium

Note from Eqs. (26) that

$$\vec{\nabla} \cdot \vec{E}_1 = - \frac{\vec{\nabla} \cdot [\vec{E}_1(\vec{\rho}, z) \Delta\epsilon(\vec{\rho}) e^{\alpha z}]}{\epsilon_1} \quad (41a)$$

and

$$\vec{\nabla} \cdot \vec{E}_2 = 0 \quad (41b)$$

may be obtained by simply taking the divergence of both sides. Applying a perturbation expansion to Eq. (41a) as

in Eq. (27b) yields

$$\vec{\nabla} \cdot \vec{E}_1^{(1)} = - \frac{\vec{\nabla} \cdot [\vec{E}_1^{(0)}(\vec{\rho}, z) \Delta \epsilon_1(\vec{\rho}) e^{\alpha z}]}{\epsilon_1} \quad (41c)$$

These results may be obtained by another approach as follows. In general, for a linear dielectric medium,

$$\vec{\nabla} \cdot \vec{E} = 4\pi \times (\text{total charge density}), \quad (42a)$$

$$\vec{\nabla} \cdot (\vec{E} + 4\pi \vec{P}) = \vec{\nabla} \cdot \vec{D} = 4\pi \times (\text{free charge density}), \quad (42b)$$

where $\vec{D} = \epsilon \vec{E}$ is a displacement vector and \vec{P} is a polarization vector. In medium 1 (Fig. 4), there are no free charges and Eq. (42b) is equal to zero. Thus, from Eq. (42b), we may write, to first order,

$$\vec{\nabla} \cdot \{[\epsilon_1 + \Delta \epsilon(\vec{\rho}, z)](\vec{E}_1^{(0)} + \vec{E}_1^{(1)})\} = 0. \quad (43)$$

Separating out the zeroth- and first-order terms and equating each to zero yields

$$\vec{\nabla} \cdot \vec{E}_1^{(0)} = 0, \quad (44a)$$

$$\vec{\nabla} \cdot \vec{E}_1^{(1)} = - \frac{\vec{\nabla} \cdot [\vec{E}_1^{(0)}(\vec{\rho}, z) \Delta \epsilon(\vec{\rho}, z)]}{\epsilon_1}, \quad (44b)$$

the latter of which agrees with Eq. (41c). From Eq. (42b),

$$[\epsilon_1 + \Delta \epsilon(\vec{\rho}, 0)] \left[E_{1z}^{(0)} + E_{1z}^{(1)} + \Delta \epsilon(\vec{\rho}, 0) \left(\frac{\partial E_{1z}^{(0)}}{\partial \epsilon} \right)_{\epsilon=\epsilon_1} \right] - \left[E_{2z}^{(0)} + E_{2z}^{(1)} + \Delta \epsilon(\vec{\rho}, 0) \left(\frac{\partial E_{2z}^{(0)}}{\partial \epsilon} \right)_{\epsilon=\epsilon_1} \right] = 0. \quad (46b)$$

Separating out the zeroth- and first-order terms and neglecting those of higher order yields

$$E_{2z}^{(0)} - \epsilon_1 E_{1z}^{(0)} = 0 \quad (46c)$$

and

$$E_{2z}^{(1)} - \epsilon_1 E_{1z}^{(1)} = \Delta \epsilon(\vec{\rho}, 0) \left[\epsilon_1 \frac{\partial E_{1z}^{(0)}}{\partial \epsilon} - \frac{\partial E_{2z}^{(0)}}{\partial \epsilon} + E_{1z}^{(0)} \right]_{\epsilon=\epsilon_1}. \quad (46d)$$

Equation (46c) is simply the standard zeroth-order result. However, Eq. (46d) implies a discontinuity in the first-order field to account for the fluctuating dielectric permittivity at the $z=0$ interface. Using the zeroth-order fields given in Eqs. (10) and (11), the right-hand side of Eq. (46d) may be evaluated explicitly. The result is zero. In other words, Eq. (46d) is identically zero and thus there is no discontinuity in the normal component of the displacement vector for the first-order fields. Equation (46d) reduces to

$$E_{2z}^{(1)} - \epsilon_1 E_{1z}^{(1)} = 0. \quad (46e)$$

The remaining boundary conditions may be computed and the equations analogous to Eq. (46d) are

$$\vec{\nabla} \cdot \vec{E}_1^{(1)} = -4\pi \vec{\nabla} \cdot \vec{P}_1^{(1)}, \quad (45a)$$

and therefore,

$$\rho_P = - \vec{\nabla} \cdot \vec{P}_1^{(1)} = \frac{\vec{\nabla} \cdot [\vec{E}_1^{(0)}(\vec{\rho}, z) \Delta \epsilon(\vec{\rho}, z)]}{4\pi \epsilon_1}, \quad (45b)$$

where ρ_P is the induced polarization charge density. Use of Eqs. (5b) and (22b) in Eqs. (41c) or (44b) yields exact agreement with Eq. (40).

D. Boundary conditions

The solutions given in Eqs. (35)–(38) are particular solutions to Eqs. (26). However, the solutions must satisfy the boundary conditions across the interface including the fluctuating dielectric permittivity. To calculate these boundary conditions to first order, by analogy with the surface-roughness calculation, we first consider as an example the continuity of the normal component of the displacement vector across the interface. Since the surface is smooth, the continuity condition at $z=0$ may be written as

$$\epsilon(\vec{\rho}, 0) \vec{E}_{1z}(\vec{\rho}, 0) - E_{2z}(\vec{\rho}, 0) = 0. \quad (46a)$$

Expanding the electric fields $E_{1z}(\vec{\rho}, 0)$ and $E_{2z}(\vec{\rho}, 0)$ about $\epsilon = \epsilon_1$ yields, at $z=0$,

$$E_{2x}^{(1)} - E_{1x}^{(1)} = \Delta \epsilon(\vec{\rho}, 0) \left[\frac{\partial E_{1y}^{(0)}}{\partial \epsilon} - \frac{\partial E_{2y}^{(0)}}{\partial \epsilon} \right]_{\epsilon=\epsilon_1} \equiv 0, \quad (46f)$$

$$E_{2y}^{(1)} - E_{1y}^{(1)} = \Delta \epsilon(\vec{\rho}, 0) \left[\frac{\partial E_{1x}^{(0)}}{\partial \epsilon} - \frac{\partial E_{2x}^{(0)}}{\partial \epsilon} \right]_{\epsilon=\epsilon_1} \equiv 0, \quad (46g)$$

$$H_{2x}^{(1)} - H_{1x}^{(1)} = \Delta \epsilon(\vec{\rho}, 0) \left[\frac{\partial H_{1x}^{(0)}}{\partial \epsilon} - \frac{\partial H_{2x}^{(0)}}{\partial \epsilon} \right]_{\epsilon=\epsilon_1} \equiv 0, \quad (46h)$$

$$H_{2y}^{(1)} - H_{1y}^{(1)} = \Delta \epsilon(\vec{\rho}, 0) \left[\frac{\partial H_{1y}^{(0)}}{\partial \epsilon} - \frac{\partial H_{2y}^{(0)}}{\partial \epsilon} \right]_{\epsilon=\epsilon_1} \equiv 0, \quad (46i)$$

$$H_{2z}^{(1)} - H_{1z}^{(1)} = \Delta \epsilon(\vec{\rho}, 0) \left[\frac{\partial H_{1z}^{(0)}}{\partial \epsilon} - \frac{\partial H_{2z}^{(0)}}{\partial \epsilon} \right]_{\epsilon=\epsilon_1} \equiv 0. \quad (46j)$$

These results are not surprising since the scattering currents in this calculation are bulk currents, not surface currents. Thus, the continuity conditions of the first-order fields satisfy the same boundary conditions as the zeroth-order fields. In fact, all higher-order terms in expanding the fields about $\epsilon = \epsilon_1$ result in the expansion coefficients of the $[\Delta \epsilon(\vec{\rho}, 0)]^n$ terms vanishing identically. Once again, this is expected since we are merely satisfying boundary conditions at a particular point regardless of the value of $\epsilon(\vec{\rho}, 0)$ at that point. This is in contrast to the calculation for the case of scattering from surface roughness. The conclusion of this section is that Eqs. (35) and

(36) are the complete solution to the scattered field in that they satisfy the appropriate wave equation and the boundary conditions. That the solutions in Eqs. (35) and (36) satisfy the boundary conditions can be seen from Eqs. (37) or (39), along with Appendix A, where the continuity conditions on $\underline{g}^{(1,1)}\underline{e}_1^{(0)}$ and $\underline{g}^{(2,1)}\underline{e}_1^{(0)}$ are discussed, or from Eqs. (35) and (36) directly.

E. Angle-resolved scattering

This section closely parallels Sec. IID. Again the time-averaged Poynting vector is calculated and integration as in Eq. (17a) is performed. The result analogous to Eq. (17b) is

$$P_d = \frac{\omega}{4(2\pi)^3} \int d^2k q_2 \frac{|\Delta\epsilon(\vec{k}_0 - \vec{k})|^2}{|q + q_1 + i\alpha|^2} (|p_{2d}|^2 + |s_{2d}|^2) \times e^{-2z \text{Im}(q_2)}, \quad (47)$$

and the differential fractional scattered power may be written as

$$\frac{1}{P_0} \left\langle \frac{dP_d}{d\Omega} \right\rangle = \frac{(\omega/c)^4 \cos^2\theta}{(2\pi)^2 \cos\theta_0} [|p_{2d}|^2 + |s_{2d}|^2] \times \frac{\langle |\Delta\epsilon(\vec{k}_0 - \vec{k})|^2 \rangle}{L^2 |q + q_1 + i\alpha|^2} \quad (48a)$$

or

$$\frac{1}{P_0} \left\langle \frac{dP_d}{d\Omega} \right\rangle = \frac{(\omega/c)^4 \cos^2\theta}{(2\pi)^2 \cos\theta_0} [|p_{2d}|^2 + |s_{2d}|^2] \times \frac{g_d(\vec{k}_0 - \vec{k})}{|q + q_1 + i\alpha|^2}, \quad (48b)$$

where the subscript d refers to dielectric fluctuation scattering. The first and second terms in the square brackets of Eqs. (48) refer to scattering which is p and s polarized, respectively, relative to the plane of scattering. Note again that the scattering is proportional to $(\omega/c)^4$ or λ^{-4} . As discussed earlier, this is characteristic of Rayleigh scattering. The ensemble average acts only on $|\Delta\epsilon(\vec{k}_0 - \vec{k})|^2$, and by analogy with Eqs. (19), we have let

$$g_d(\vec{k}_0 - \vec{k}) = \frac{\langle |\Delta\epsilon(\vec{k}_0 - \vec{k})|^2 \rangle}{L^2}, \quad (49a)$$

where $g_d(\vec{k}_0 - \vec{k})$ is the two-dimensional Fourier transform of the autocovariance function of dielectric fluctuations $G_d(\vec{\tau}) = \langle \Delta\epsilon(\vec{\rho})\Delta\epsilon(\vec{\rho} + \vec{\tau}) \rangle$, or

$$g_d(\vec{K}) = \int d^2\tau G_d(\vec{\tau}) e^{i\vec{K} \cdot \vec{\tau}}, \quad (49b)$$

where $G_d(0) = \xi_d^2$ is the mean-square deviation of the dielectric perturbation about ϵ_1 .

F. Polarization ratio

By analogy with Sec. IIE, for $\phi=0$ or π , the p -polarized to s -polarized ratio in the scattered field can be written from Eqs. (48), (11e), and (11f) as

$$\xi_d = \left\langle \frac{dP_d^p}{dP_d^s} \right\rangle = \frac{|qq_1 \cos\phi - kk_0|^2 |q_1 + q_2|^2 |q + q_0|^2}{(\omega/c)^4 |q_2\epsilon_1 + q_1|^2 |q + q_0\epsilon_1|^2}, \quad (50)$$

where the superscripts p and s refer to p or s polarization. Note that this ratio depends on the polar angle θ as well as on ϵ_1 . The ratio ξ_d is different than the corresponding surface roughness ratio ξ_r of Eq. (21). The ratio ξ_r/ξ_d is

$$\frac{\xi_r}{\xi_d} = \frac{|qq_1 \cos\phi - kk_0\epsilon_1|^2}{|qq_1 \cos\phi - kk_0|^2}. \quad (51)$$

For normal incidence ($k_0=0$) or if $k_0 \neq 0$, for scattering normal to the surface ($k=0$), the ratio in Eq. (51) is unity.

G. Physical differences between roughness and dielectric scattering

As mentioned above, in the event k_0 vanishes (normal incidence), the scattering coefficients p_{2r} and p_{2d} for roughness and dielectric scattering become identical. This is evident in Eqs. (36b) and (15e). The scattering coefficients s_{2r} and s_{2d} are identical regardless of the value of k_0 . However, this is not to say that the scattering intensities are the same for both types of scattering. When k_0 vanishes, this is equivalent to the z component of the incident electric field being zero. Since the source currents responsible for scattered light for both roughness and dielectric scattering are proportional to the direction of the incident electric field vector, it follows that the z components of the source currents generate scattering in a physically different manner for the roughness and dielectric scattering processes. This physical difference lies in the fact that for dielectric scattering the source currents are in the lower medium, and to be observed in the upper medium, the radiation emanating from these currents must pass from the lower medium, through the boundary, into the upper medium. In the case of roughness scattering, a Green's-function approach may also be used which would make this calculation more analogous to the dielectric scattering calculation done here. As discussed more extensively elsewhere,⁸ for the case of roughness scattering the scattering currents are located at the interface between media 1 and 2. These currents are proportional to a Dirac δ function which constrains the currents to be at the $z=0$ boundary. This is in contrast to the dielectric scattering case where the scattering currents are throughout the bulk of medium 1. Since the roughness currents are at the boundary, there is an ambiguity in the placement and strength of the scattering currents. The ambiguity comes in how to approach the boundary, i.e., from the lower or upper medium, and whether to use the z component of the electric field from medium 1 or 2 since they are discontinuous across the boundary. It turns out that when using the Green's function calculated in the manner described in

this work and in Ref. 11, it is necessary to use source currents which are proportional to the incident electric field in medium 1 (evaluated at $z=0$), but which are placed in and approach the boundary from the medium-2 side. With this in mind, it is clear that both roughness

and dielectric scattering dipole currents are driven by the electric field in medium 1, but the difference lies in the fact that the dielectric currents radiate *through* the boundary and the roughness currents radiate *from* the boundary. This leads to the differences in p_{2r} and p_{2d} .

IV. SCATTERING FROM SURFACE ROUGHNESS PLUS DIELECTRIC FLUCTUATIONS

Consider now a linear superposition of Eqs. (13b) and (36a) to yield the first-order electric field caused by scattering from surface roughness plus dielectric fluctuations. The electric field solution may be written as

$$\vec{E}_2^{(1)}(\vec{\rho}, z) = - \left[\frac{1}{2\pi} \right]^2 \int d^2k [(\hat{k}q_2 - \hat{z}k)M(\vec{k}_0 - \vec{k}) + (\hat{k} \times \hat{z})(\omega/c)N(\vec{k}_0 - \vec{k})] e^{i(\vec{k} \cdot \vec{\rho} + q_2 z)}, \quad (52a)$$

whereas the magnetic field is

$$\vec{H}_2^{(1)}(\vec{\rho}, z) = - \left[\frac{1}{2\pi} \right]^2 \int d^2k [(\hat{k}q_2 - \hat{z}k)N(\vec{k}_0 - \vec{k}) - (\hat{k} \times \hat{z})(\omega/c)M(\vec{k}_0 - \vec{k})] e^{i(\vec{k} \cdot \vec{\rho} + q_2 z)}, \quad (52b)$$

where

$$M(\vec{k}_0 - \vec{k}) = i(1 - \epsilon_1)p_{2r}\Delta z(\vec{k}_0 - \vec{k}) + p_{2d} \left[\frac{\Delta\epsilon(\vec{k}_0 - \vec{k})}{q + q_1 + i\alpha} \right] \quad (52c)$$

and

$$N(\vec{k}_0 - \vec{k}) = i(1 - \epsilon_1)s_{2r}\Delta z(\vec{k}_0 - \vec{k}) + s_{2d} \left[\frac{\Delta\epsilon(\vec{k}_0 - \vec{k})}{q + q_1 + i\alpha} \right]. \quad (52d)$$

This superposition shows that the fields scattered from roughness and dielectric fluctuations have similar forms. Calculation of the energy flow away from the interface in the positive z direction yields

$$P_{rd} = \frac{\omega}{4(2\pi)^3} \int d^2k q_2 [|M(\vec{k}_0 - \vec{k})|^2 + |N(\vec{k}_0 - \vec{k})|^2], \quad (53a)$$

and for the ensemble average of the fractional scattered power, we have

$$\frac{1}{P_0} \left\langle \frac{dP_{rd}}{d\Omega} \right\rangle = \frac{(\omega/c)^4 \cos^2 \theta}{(2\pi)^3 \cos \theta_0 L^2} [\langle |M(\vec{k}_0 - \vec{k})|^2 \rangle + \langle |N(\vec{k}_0 - \vec{k})|^2 \rangle]. \quad (53b)$$

The terms in the square brackets represent p - and s -polarized scattered power, respectively. As was done previously, the p -polarized to s -polarized ratio is

$$\xi_{rd} = \frac{\langle |M(\vec{k}_0 - \vec{k})|^2 \rangle}{\langle |N(\vec{k}_0 - \vec{k})|^2 \rangle}. \quad (54)$$

The major difference of ξ_{rd} as compared to ξ_r and ξ_d is that ξ_{rd} depends on the statistical properties of the random variables $\Delta z(\vec{\rho})$ and $\Delta\epsilon(\vec{\rho})$. This is seen clearly in expanding $\langle |M(\vec{k}_0 - \vec{k})|^2 \rangle$ and $\langle |N(\vec{k}_0 - \vec{k})|^2 \rangle$. We find that

$$\begin{aligned} \langle |M(\vec{k}_0 - \vec{k})|^2 \rangle = & \left[|1 - \epsilon_1|^2 |p_{2r}|^2 \frac{\langle |\Delta z(\vec{k}_0 - \vec{k})|^2 \rangle}{L^2} + \frac{|p_{2d}|^2 \langle |\Delta\epsilon(\vec{k}_0 - \vec{k})|^2 \rangle}{|q + q_1 + i\alpha|^2 L^2} \right. \\ & \left. + 2 \operatorname{Re} \left[\frac{i(1 - \epsilon_1)p_{2r}p_{2d}^* \langle \Delta z(\vec{k}_0 - \vec{k}) \Delta\epsilon^*(\vec{k}_0 - \vec{k}) \rangle}{(q + q_1 + i\alpha)^* L^2} \right] \right], \end{aligned} \quad (55a)$$

or, with Eqs. (19a) and (49a),

$$\langle |M(\vec{k}_0 - \vec{k})|^2 \rangle = \left[|1 - \epsilon_1|^2 |p_{2r}|^2 g_r(\vec{k}_0 - \vec{k}) + \frac{|p_{2d}|^2}{|q + q_1 + i\alpha|^2} g_d(\vec{k}_0 - \vec{k}) + 2 \operatorname{Re} \left[\frac{i(1 - \epsilon_1)p_{2r}p_{2d}^* g_{rd}(\vec{k}_0 - \vec{k})}{(q + q_1 + i\alpha)^*} \right] \right], \quad (55b)$$

where * denotes complex conjugate. The $\langle |N(\vec{k}_0 - \vec{k})|^2 \rangle$ term is identical to Eqs. (55) with p_{2r} and p_{2d} replaced by s_{2r} and s_{2d} , respectively. There are several interesting new features regarding $\langle dP_{rd}/d\Omega \rangle / P_0$ with these expressions for $\langle |M(\vec{k}_0 - \vec{k})|^2 \rangle$ and $\langle |N(\vec{k}_0 - \vec{k})|^2 \rangle$. First, there is the term

$$g_{rd}(\vec{k}_0 - \vec{k}) = \frac{\langle \Delta z(\vec{k}_0 - \vec{k}) \Delta \epsilon^*(\vec{k}_0 - \vec{k}) \rangle}{L^2}, \quad (56)$$

which describes the cross-power spectral density associated with the cross correlation between the random variables $\Delta z(\vec{\rho})$ and $\Delta \epsilon(\vec{\rho})$. This term would be zero if the random variables in question were statistically independent (uncorrelated). On the other hand, if there is a connection between the surface roughness $\Delta z(\vec{\rho})$ variations and the dielectric permittivity fluctuations $\Delta \epsilon(\vec{\rho})$, then the cross correlation will not vanish. By analogy with Eqs. (19b) and (49b), we write

$$g_{rd}(\vec{K}) = \int d^2\tau G_{rd}(\vec{\tau}) e^{i\vec{K} \cdot \vec{\tau}}, \quad (57)$$

where

$$G_{rd}(\vec{\tau}) = \langle \Delta z(\vec{\rho}) \Delta \epsilon(\vec{\rho} + \vec{\tau}) \rangle$$

is the cross-correlation function. Since the $\Delta \epsilon(\rho)$ is a dielectric permittivity, which may be complex, it follows that $g_{rd}(\vec{k}_0 - \vec{k})$ and $G_{rd}(\tau)$ may be complex. General properties of cross-correlation and cross-power-spectral-density functions are given by Bendat and Piersol.¹²

The effect of the interference term in Eqs. (55) depends on several factors. These include the choice for g_{rd} and the magnitude and sign of the real part of the expression in the large parentheses. Since g_{rd} can be complex, the choice with regard to its real and imaginary parts can be an important one as to the effect on the overall scattering.

It is not possible to measure $G_d(\vec{\tau})$ and $G_{rd}(\vec{\tau})$, but experimental measurements of the roughness factor $G_r(\vec{\tau})$ have been made. In this paper, we will make reasonable guesses for $G_d(\vec{\tau})$ and $G_{rd}(\vec{\tau})$ in order to generate numerical results.

V. NUMERICAL RESULTS

A. Autocovariance, cross covariance, and power spectral-density functions

In order to obtain numerical results and get some feeling for the potential importance of including dielectric fluctuations as a scattering mechanism, we will make the following assumptions regarding the autocovariance and cross-correlation functions. We have used two-part autocovariance functions¹ for $G_r(\vec{\tau})$, $G_d(\vec{\tau})$, and $G_{rd}(\vec{\tau})$. For $G_r(\vec{\tau})$ and $G_d(\vec{\tau})$, we assume a combination of exponential and Gaussian forms as

$$G_r(\vec{\tau}) = G_{rL}(\vec{\tau}) + G_{rS}(\vec{\tau}) = \zeta_{rL}^2 \exp\left[-\frac{|\tau|}{\sigma_{rL}}\right] + \zeta_{rS}^2 \exp\left[-\left[\frac{\tau}{\sigma_{rS}}\right]^2\right] \quad (58a)$$

and

$$G_d(\vec{\tau}) = G_{dL}(\vec{\tau}) + G_{dS}(\vec{\tau}) = \zeta_{dL}^2 \exp\left[-\frac{|\tau|}{\sigma_{dL}}\right] + \zeta_{dS}^2 \exp\left[-\left[\frac{\tau}{\sigma_{dS}}\right]^2\right], \quad (58b)$$

where the subscripts L and S refer to long- and short-range parameters, respectively. The long-range σ values are correlation lengths greater than λ and mainly contribute to scattering in the near-specular direction. The short-range values are correlation lengths less than λ and contribute to large-angle scattering. Note that the autocovariance functions are isotropic since they do not depend on the direction of $\vec{\tau}$, where $\vec{\tau} = |\vec{\tau}|$. As before, r and d refer to roughness and dielectric contributions, respectively. The ζ refers to rms values. The form of Eq. (58a) is chosen because of physical reasons and previous success in fitting scattering data and theory.¹ The physical basis of Eqs. (58) is as follows. Since the short-range parameters describe the correlation properties for small τ values, the short-range autocovariance function must have a zero slope as $\tau \rightarrow 0$. This is to avoid an unphysical infinite mean-square slope of the surface roughness which occurs for autocovariance functions which have nonzero slopes at the origin. Thus, a Gaussian form is chosen for the short-range autocovariance function. An exponential form is chosen for the long-range autocovariance function because exponential autocovariance functions have been measured many times for surface roughness.¹³ Even though exponential autocovariance functions have nonzero slopes for $\tau=0$, the experimental measurements can easily be physically realistic since the lateral resolution of surface-profiling instruments is on the order of 0.1 μm or greater. Thus the profiling instrument cannot address the region where $\tau \rightarrow 0$. Finally, experience has shown that the short-range rms parameter ζ_{rS} is dominant over the long-range parameter ζ_{rL} in the vicinity of $\tau \rightarrow 0$, so that the effect of the exponential autocovariance function is minimized.

Considering the cross-correlation properties of the statistical variables, we assume four different situations which will be called cases 1, 2, 3, and 4. Separating $\Delta \epsilon$ into its real and imaginary parts, the general form of the cross-correlation function is written here as

$$G_{rd}(\vec{\tau}) = \langle \Delta z(\vec{\rho}) \text{Re}[\Delta \epsilon(\vec{\rho} + \vec{\tau})] \rangle + i \langle \Delta z(\vec{\rho}) \text{Im}[\Delta \epsilon(\vec{\rho} + \vec{\tau})] \rangle = |G_{rd}(\vec{\tau})| e^{i\delta_{rd}}, \quad (58c)$$

where $\langle \dots \rangle$ denotes an ensemble average. The term δ_{rd} is an average phase which depends on the cross correlation between $\Delta z(\vec{\rho})$ and $\Delta \epsilon(\vec{\rho})$ as

$$\delta_{rd} = \tan^{-1} \left[\frac{\langle \Delta z(\vec{\rho}) \text{Im}[\Delta \epsilon(\vec{\rho} + \vec{\tau})] \rangle}{\langle \Delta z(\vec{\rho}) \text{Re}[\Delta \epsilon(\vec{\rho} + \vec{\tau})] \rangle} \right]. \quad (58d)$$

The phase of $\Delta z(\vec{\rho})$ is 0 or π , depending on the sign of $\Delta z(\vec{\rho})$. $\Delta \epsilon(\vec{\rho} + \vec{\tau})$, which is complex, has a phase which ranges from 0 for $\Delta \epsilon(\vec{\rho} + \vec{\tau})$ real and positive to π for

$\Delta\epsilon(\vec{\rho} + \vec{\tau})$ real and negative. Phase values between 0 and π indicate a nonzero, positive imaginary part of $\Delta\epsilon(\vec{\rho} + \vec{\tau})$. With these possible phase values for $\Delta z(\vec{\rho})$ and $\Delta\epsilon(\vec{\rho} + \vec{\tau})$, the term δ_{rd} may take on values ranging from 0 to 2π . For simplicity, Eq. (58c) is assumed to have the analytic form

$$G_{rd}(\vec{\tau}) = C \left\{ \zeta_{rL} \zeta_{dL} \exp \left[-\frac{|\tau|}{2} \left(\frac{1}{\sigma_{rL}} + \frac{1}{\sigma_{dL}} \right) \right] + \zeta_{rS} \zeta_{dS} \exp \left[-\frac{\tau^2}{2} \left(\frac{1}{\sigma_{rS}^2} + \frac{1}{\sigma_{dS}^2} \right) \right] \right\}. \quad (58e)$$

where the coefficient C represents $\exp(i\delta_{rd})$ in Eqs. (58c). This expression assumes that the long- and short-range parts of the cross-correlation functions are a phenomenological blend of the autocovariance functions $G_r(\vec{\tau})$ and $G_d(\vec{\tau})$, and have functional forms proportional to $[G_{rL}(\vec{\tau})G_{dL}(\vec{\tau})]^{1/2}$ and $[G_{rS}(\vec{\tau})G_{dS}(\vec{\tau})]^{1/2}$, respectively. We assume four different choices for the complex value of $C = a + ib$, which are called cases 1, 2, 3, and 4. The coefficients (a, b) are

$$C = (0, 0) \quad (\text{case 1}), \quad (59a)$$

$$C = (0, 1) = i \quad (\text{case 2}), \quad (59b)$$

$$C = (-1, 0) \quad (\text{case 3}), \quad (59c)$$

and

$$C = (1, 0) \quad (\text{case 4}), \quad (59d)$$

Case 1 assumes that the cross correlation is zero, which implies that the variables $\Delta z(\vec{\rho})$ and $\Delta\epsilon(\vec{\rho})$ are independent,

and thus there is no statistical connection between the roughness and the dielectric variations. This is equivalent to saying that the phase δ_{rd} fluctuates in such a way that the ensemble average vanishes. Cases 2, 3, and 4 consider nonvanishing cross correlation. Case 2 assumes that the variables $\Delta z(\vec{\rho})$ and $\Delta\epsilon(\vec{\rho} + \vec{\tau})$ are, on the average, out of phase by $\delta_{rd} = \pi/2$. From Eq. (58d), this implies that the denominator $\langle \Delta z(\vec{\rho}) \text{Re}[\Delta\epsilon(\vec{\rho} + \vec{\tau})] \rangle$ vanishes. In other words, there is no correlation between the $\Delta z(\vec{\rho})$ and the real part of $\Delta\epsilon(\vec{\rho})$, but there is correlation between $\Delta z(\vec{\rho})$ and the imaginary part of $\Delta\epsilon(\vec{\rho})$. It seems unlikely that the real and imaginary parts of $\Delta\epsilon(\vec{\rho})$ would be independent unless one of the two parts were negligible. Thus it is likely that, for case 2, $\Delta\epsilon(\vec{\rho})$ is essentially a pure imaginary number and models an absorptive perturbation. Case 2 is inspired as a result of experimental evidence of increased absorption (in the form of decreased reflectance) at Ag interfaces as compared to bulk absorption.¹⁴ Case 3 assumes that the phase angle is π . Therefore, $\langle \Delta z(\vec{\rho}) \text{Im}[\Delta\epsilon(\vec{\rho})] \rangle$ vanishes (or at least is negligible compared to $\langle \Delta z(\vec{\rho}) \text{Re}[\Delta\epsilon(\vec{\rho})] \rangle$), and signwise the $\text{Re}(\Delta\epsilon)$ fluctuates oppositely to that of $\Delta z(\vec{\rho})$. It follows that if $\Delta\epsilon$ is essentially real, then when Δz is positive, $\Delta\epsilon$ is negative and vice versa. Finally, case 4 assumes that the phase angle δ_{rd} is zero. Thus, the major difference between case 4 and case 3 is that the variables Δz and $\Delta\epsilon$ fluctuate with the same sign for case 4. Therefore it may be said that Δz and $\Delta\epsilon$ are anticorrelated and positively correlated for cases 3 and 4, respectively. These four cases will provide some indication of the relative importance of the cross-correlation properties of the surface.

The power-spectral-density functions associated with the autocovariance functions in Eqs. (58a) and (58b) are

$$g_r(\vec{k}_0 - \vec{k}) = \frac{2\pi \zeta_{rL}^2 \sigma_{rL}^2}{(1 + |\vec{k}_0 - \vec{k}|^2 \sigma_{rL}^2)^{3/2}} + \pi \zeta_{rS}^2 \sigma_{rS}^2 \exp\left[-\frac{1}{4}(|\vec{k} - \vec{k}_0|^2 \sigma_{rS}^2)\right] \quad (60a)$$

and

$$g_d(\vec{k}_0 - \vec{k}) = \frac{2\pi \zeta_{dL}^2 \sigma_{dL}^2}{(1 + |\vec{k}_0 - \vec{k}|^2 \sigma_{dL}^2)^{3/2}} + \pi \zeta_{dS}^2 \sigma_{dS}^2 \exp\left[-\frac{1}{4}(|\vec{k} - \vec{k}_0|^2 \sigma_{dS}^2)\right], \quad (60b)$$

respectively. The cross-power-spectral-density function associated with Eq. (58e) is

$$g_{rd}(\vec{k}_0 - \vec{k}) = C^* \left[\frac{2\pi \zeta_{rdL}^2 \sigma_{rdL}^2}{(1 + |\vec{k}_0 - \vec{k}|^2 \sigma_{rdL}^2)^{3/2}} + \pi \zeta_{rdS}^2 \sigma_{rdS}^2 \exp\left[-\frac{1}{4}(|\vec{k} - \vec{k}_0|^2 \sigma_{rdS}^2)\right] \right], \quad (60c)$$

where

$$\zeta_{rdL} = (\zeta_{rL} \zeta_{dL})^{1/2}, \quad (60d)$$

$$\zeta_{rdS} = (\zeta_{rS} \zeta_{dS})^{1/2}, \quad (60e)$$

$$\sigma_{rdL} = \frac{2\sigma_{rL} \sigma_{dL}}{\sigma_{rL} + \sigma_{dL}}, \quad (60f)$$

and

$$\sigma_{rdS} = \frac{\sigma_{rS} \sigma_{dS}}{[(\sigma_{rS}^2 + \sigma_{dS}^2)/2]^{1/2}}. \quad (60g)$$

Note that in Eq. (60c) the C coefficient is its complex conjugate, to be consistent with Eq. (56). Since both the surface-

roughness and dielectric fluctuations are assumed to be isotropic, the power-spectral-density functions in Eqs. (60a)–(60c) are independent of the direction of $\vec{k}_0 - \vec{k}$, where $|\vec{k}_0 - \vec{k}|^2 = k_0^2 + k^2 - 2kk_0 \cos\phi$.

B. Numerical analysis of theoretical results

The numerical results in this section have been obtained from Eqs. (18b), (48b), and (53b) using the various power-spectral-density functions described above. In all the numerical examples, the inhomogeneous medium is assumed to be silver with $\epsilon_1 = (-16.4, 0.53)$ at $\lambda = 0.6328 \mu\text{m}$; the angle of incidence $\theta_0 = 60^\circ$, and scattering is confined to the plane of incidence. Table II summarizes various statistical parameters ζ and σ which have been used in the calculations. The correlation lengths for the roughness and dielectric fluctuations are assumed to be identical, and the rms roughness values, which are typical of measured values, are assumed to be the same for all the numerical examples. The parameters which were varied in the analysis were the rms values of the dielectric fluctuations. Except for case 1, the cross-correlation parameters were calculated from Eqs. (60d)–(60g) and are given in Table II.

The polarization ratio of the scattered light is, from Eq. (54),

$$\xi_{rd} = \frac{\left| |1 - \epsilon_1|^2 |p_{2r}|^2 g_r(\vec{k}_0 - \vec{k}) + \frac{|p_{2d}|^2}{|q + q_1 + i\alpha|^2} g_d(\vec{k}_0 - \vec{k}) + 2 \operatorname{Re} \left[\frac{i(1 - \epsilon_1) p_{2r} p_{2d}^* g_{rd}(\vec{k}_0 - \vec{k})}{(q + q_1 + i\alpha)^*} \right] \right|}{\left| |1 - \epsilon_1|^2 |s_{2r}|^2 g_r(\vec{k}_0 - \vec{k}) + \frac{|s_{2d}|^2}{|q + q_1 + i\alpha|^2} g_d(\vec{k}_0 - \vec{k}) + 2 \operatorname{Re} \left[\frac{i(1 - \epsilon_1) s_{2r} s_{2d}^* g_{rd}(\vec{k}_0 - \vec{k})}{(q + q_1 + i\alpha)^*} \right] \right|}. \quad (61)$$

For case 1, the g_{rd} term vanishes and the interference term is omitted. For cases 2, 3, and 4, the g_{rd} term is nonzero and the interference term is not omitted. In Eq. (61) it is evident that the ratio ξ_{rd} generally depends on the statistical properties of the roughness and dielectric fluctuations with or without cross correlation between the random variables.

If the perturbation ratios are set equal so that $\zeta_r/\lambda = \zeta_d/|\epsilon_1|$, then the roughness scattering is several orders of magnitude greater than the dielectric scattering and the latter can be neglected. Thus, it is clear that the magnitudes of the rms dielectric values must be considerably larger than the corresponding rms roughness values in order for dielectric scattering to contribute. In the fol-

lowing numerical results, the rms dielectric values have been chosen such that the $\zeta_d/|\epsilon_1|$ ratio is 1 to 2 orders of magnitude larger than the ζ_r/λ ratio. Even with such increased rms dielectric parameters, it will be seen that the magnitude of the dielectric scattering is still much smaller than that of the corresponding roughness scattering. However, interferences between the two fields, using the types of cross-correlation functions chosen here, leads to significant differences between the scattering intensity predicted by roughness alone and roughness plus dielectric fluctuations.

Figure 5 pertains to data set 1. The rms dielectric values are $\zeta_{dL} = 0.2$ and $\zeta_{dS} = 1.0$, which yields a ratio

TABLE II. Summary of the two different sets of data for the various statistical parameters used in the numerical analysis. Note that the rms roughnesses and all correlation lengths are constant for all two data sets. The quantities ζ_r and ζ_d are defined by $(\zeta_{rL}^2 + \zeta_{rS}^2)^{1/2}$ and $(\zeta_{dL}^2 + \zeta_{dS}^2)^{1/2}$, respectively. The pertinent perturbation ratios ζ_r/λ and $\zeta_d/|\epsilon_1|$ are also shown.

Statistical parameter	Data set 1	Data set 2
ζ_{rL}	0.001 μm	0.001 μm
ζ_{rS}	0.003 μm	0.003 μm
ζ_r/λ	0.005	0.005
σ_{rL}	2.0 μm	2.0 μm
σ_{rS}	0.1 μm	0.1 μm
ζ_{dL}	0.2	0.5
ζ_{dS}	1.0	2.5
$\zeta_d/ \epsilon_1 $	0.062	0.155
σ_{dL}	2.0 μm	2.0 μm
σ_{dS}	0.1 μm	0.1 μm
ξ_{rdL}	0.014 $(\mu\text{m})^{1/2}$	0.022 $(\mu\text{m})^{1/2}$
ξ_{rdS}	0.055 $(\mu\text{m})^{1/2}$	0.087 $(\mu\text{m})^{1/2}$
σ_{rdL}	2.0 μm	2.0 μm
σ_{rdS}	0.1 μm	0.1 μm

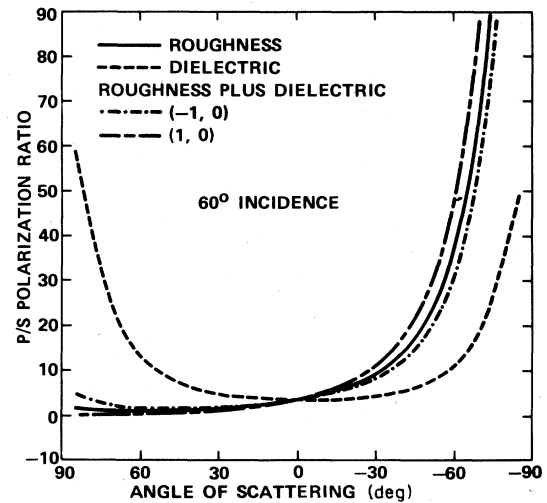


FIG. 5. Comparison of p to s polarization ratio in the plane of incidence, versus polar angle of scattering, for roughness-only, dielectric-only, and roughness plus dielectric scattering for cases 1–4. The angle of incidence is 60° and the scattering medium is Ag with $\epsilon_1 = (-16.4, 0.53)$ at $\lambda = 0.6328 \mu\text{m}$. These data were generated with data set 1.

$\xi_d/|\epsilon_1|=0.06$ and the parameter $\alpha=0.5 \mu\text{m}^{-1}$. The p to s polarization ratio is shown versus polar scattering angle θ for scattering due to roughness only, dielectric only, and roughness plus dielectric scattering for cases 1–4. Thus there are six plots in all. Note that the ratios for roughness only and dielectric only are quite different in character. The case-1 and -2 curves are essentially coincident with the roughness-only curve. Since these C values are (0,0) and (0,1), respectively, this indicates that the p to s ratio for roughness plus dielectric curves is insensitive to the imaginary part of the autocovariance function $G_{rd}(\vec{r})$ compared to the roughness-only curve. Thus, for these C values there are no predicted differences in the p to s ratio between different sample measurements. The reason for this is that the dielectric direct scattering and the interference terms [the last two terms of Eq. (61) for cases 1 and 2, respectively, in the numerator and denominator] are negligible compared to the roughness direct scattering term [first term of Eq. (61), in the numerator and denominator]. On the other hand, the case-3 and -4 curves do deviate from the roughness-only curve. For case 3, $C=(-1,0)$, and the p to s ratio is greater and lower than the ratio of the roughness-only curve in the forward scattering and retroscattering regions, respectively. For case 4, where $C=(1,0)$, the preceding pattern is reversed. In cases 3 and 4, the real part of C goes from -1 to 1 . For cases where the real part of C is nonzero, the interference term can be non-trivial compared to the roughness term and therefore contribute significantly to the overall scattering. It follows that compared to the roughness only p to s ratio in the retroscattering region, the ratio due to roughness plus dielectric scattering is decreased when the real part of $G_{rd}(\vec{r})$ is negative and increased when the real part is positive. This conclusion is, of course, to some degree based on the analytic form chosen for the cross-correlation function. As seen in Table I, the $(p \rightarrow p)/(s \rightarrow s)$ ratios are generally less than the roughness only ratio is 36.2. This would imply that the real part of $G_{rd}(\vec{r})$ is negative or that the Δz and $\Delta\epsilon$ variables are anticorrelated or fluctuate with opposite sign.

Figure 6 parallels Fig. 5, except that data set 2 is used.

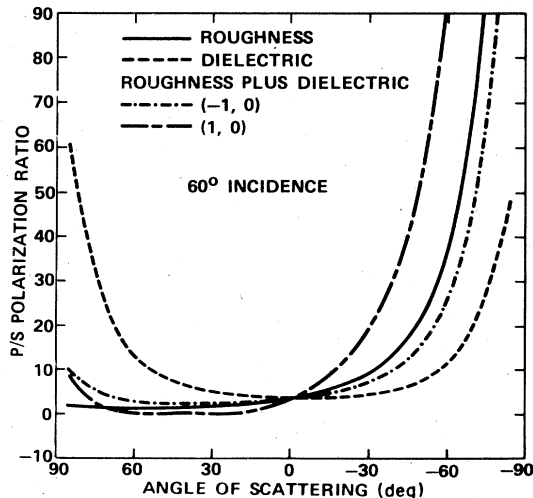


FIG. 6. Same as Fig. 5, except that data set 2 was used.

For these data, $\xi_{dL}=0.5$ and $\xi_{dS}=2.5$, which yields a ratio $\xi_d/|\epsilon_1|=0.16$. Discussions of Fig. 6 is quite analogous to Fig. 5, except that the increased dielectric parameters accentuate the effect of dielectric perturbations. The increased rms dielectric values cause the case-3 and -4 curves to be further deviated from the roughness-only curve, whereas the case-1 and -2 curves are again coincident with the roughness-only curve.

Figure 7 and 8 pertain to data set 1. These plots are the predicted angle-resolved scattering in the plane of incidence versus polar angle of scattering. These figures have plots for roughness only, dielectric only, and roughness plus dielectric scattering for cases 1–4. Considering first Fig. 7, which is for p -polarized incident and scattered light, the plots for cases 1 and 2 are coincident with the roughness-only curve. Note that the dielectric-only scattering intensity is generally much less than the roughness-only intensity. Since cases 1 and 2 are essentially identical to the roughness plot, this again says that if the real part of the cross-correlation function G_{rd} averages to zero, then $\Delta\epsilon(\vec{\rho})$ has very little effect on the scattering intensity. Furthermore, case 3 indicates that when the real part of the cross-correlation function is negative [which, for the assumptions in this work, implies anticorrelation between $\Delta z(\vec{\rho})$ and $\Delta\epsilon(\vec{\rho})$, as discussed earlier in connection with case 3], the intensity for roughness plus dielectric scattering is increased over roughness-only scattering. In addition, case 4 indicates that when the real part of the cross-correlation function is positive [which implies positive correlation between $\Delta z(\vec{\rho})$ and $\Delta\epsilon(\vec{\rho})$], the resultant intensity is less than that of roughness-only theory. Note that for case 4 a trough appears between scattering angles at 60° and 0° . In addition, the specular

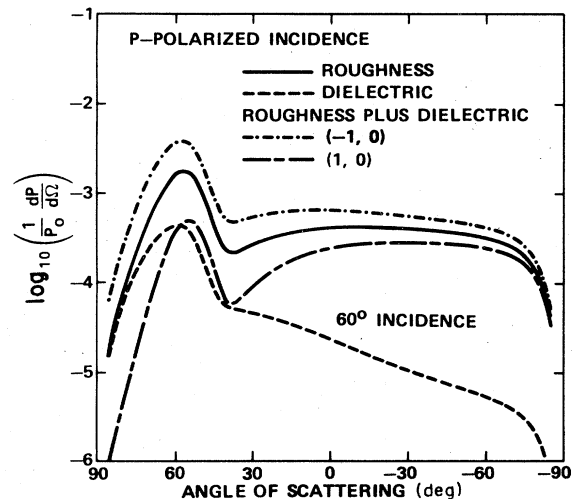


FIG. 7. Comparison of angle-resolved scattering from roughness-only, dielectric-only, and roughness plus dielectric scattering for cases 1–4. The plots are angle-resolved scattering, in the plane of incidence, versus polar scattering angle θ . The incident plane wave is p polarized at polar angle $\theta_0=60^\circ$ measured from the normal. The scattering medium is Ag with $\epsilon_1=(-16.4, 0.53)$ at $\lambda=0.6328 \mu\text{m}$. These data pertain to data set 1.

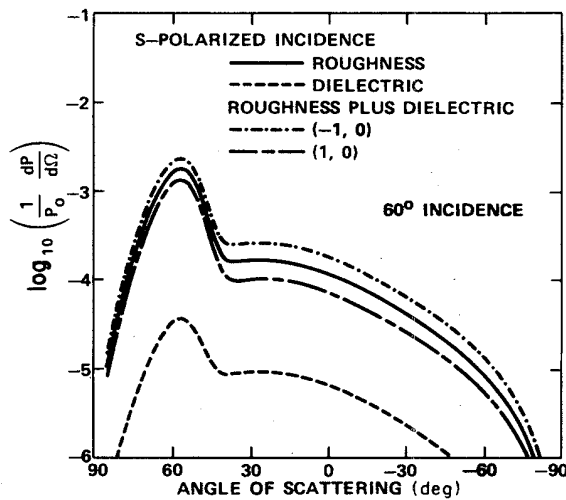


FIG. 8. Same as Fig. 7, except the incident and scattered fields are *s* polarized.

scattering is considerably depressed around the specular region, compared to the roughness-only plot. Figure 8 parallels Fig. 7, except that the incident and scattered light are *s* polarized. The trend of these data is mostly analogous to the *p*-polarized data of Fig. 7. The dielectric-only scattering is about 1 order of magnitude less than the roughness-only scattering. Cases 1 and 2 are coincident with the roughness-only curve. Cases 3 and 4 are elevated and depressed, respectively, compared to the roughness-only curve.

Figures 9 and 10 pertain to data set 2 and, analogous to Figs. 7 and 8, show the predicted angle-resolved scattering versus angle of scattering. In many respects, these plots are similar to Figs. 7 and 8, and, in fact, the roughness-only curves are unchanged. The dielectric-only curves are elevated by a factor of 6.25, compared to Figs. 7 and 8, due to the increased rms dielectric parameters. In both Figs. 9 and 10, cases 1 and 2 are again coincident with the roughness-only curve. In Fig. 9, for *p*-polarized incident and scattered light, the case-3 curve greatly resembles the

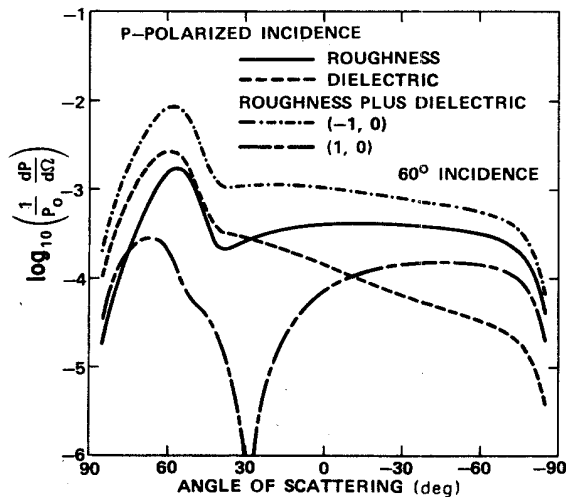


FIG. 9. Same as Fig. 7, except that data set 2 was used.

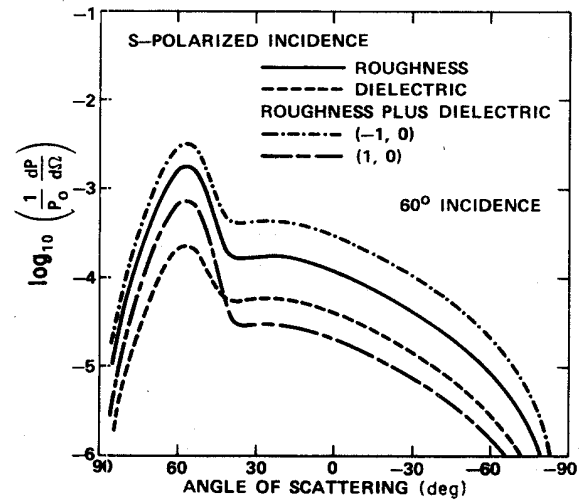


FIG. 10. Same as Fig. 8, except that data set 2 was used.

corresponding curve in Fig. 7. However, the case-4 curve of Fig. 9 is much different than the corresponding curve of Fig. 7. This is because the "trough," mentioned in connection with Fig. 7, is very much accentuated in Fig. 9. This trough is an artifact of the choice of cross-correlation function associated with case 4 and may not be an effect which would be seen experimentally. Furthermore, the experimental evidence of Table I seems to favor case 3. For this case, the trough does not materialize. In Fig. 10, for *s*-polarized incident and scattered light, the pattern is somewhat similar to Fig. 8. However, the case-4 curve is now lower, in the retroscattering region, than the dielectric-only curve. Note that there are no trough associated with the case-4 curves for *s*-polarized light in Figs. 8 and 10.

VI. CONCLUSIONS

Based on the autocovariance functions and four types of cross-correlation functions chosen in this paper and on the type of dielectric perturbation model used here, the following conclusions can be drawn.

When compared to the theoretical roughness-only *p* to *s* ratio, the polarization ratio of the scattered field due to roughness plus dielectric perturbations may or may not be sensitive to the nature of the cross correlation between the roughness and dielectric perturbations. In the numerical analysis of this work, the theory of scattering due to roughness plus dielectric perturbations is essentially the same as the roughness-only theory when the real part of the cross-correlation function G_{rd} , and consequently, the cross-power spectral density g_{rd} , is negligible. This condition could occur even though the real part of $\Delta\epsilon(\vec{\rho})$ is not negligible, provided there is no correlation between $\Delta z(\vec{\rho})$ and $\text{Re}[\Delta\epsilon(\vec{\rho})]$. However, in that case, it is most likely that the $\Delta\epsilon(\vec{\rho})$ is pure imaginary in nature. When $\text{Re}(G_{rd})$, and consequently $\text{Re}(g_{rd})$, is not negligible, it is seen that the *p* to *s* ratio may vary considerably from that predicted by roughness-only theory. When the sign of $\text{Re}(G_{rd})$ is positive (negative), the *p* to *s* ratio in the retroscattering region is increased (decreased) relative to

roughness-only theory. On the other hand, when the sign of $\text{Re}(G_{rd})$ is positive (negative), the overall scattering is decreased (increased) relative to the prediction of roughness-only scattering theory.

The intensity and shape of the angle-resolved scattered field due to (1) roughness, (2) dielectric, or (3) roughness plus dielectric perturbations can be very different. For the rms parameters chosen in this work, the intensity of angular scattering due to dielectric perturbations is seen to be at least an order of magnitude less than scattering due to roughness perturbations. When scattering due to roughness plus dielectric perturbations is considered, the resultant scattering intensity is seen to be greater than, the same as, or less than that due to roughness perturbation alone. The deciding factor lies in the choice of cross correlation and the phase relationship between the roughness and dielectric perturbations.

Of particular interest is the prediction that the ARS and the polarization ratio can be much different for scattering from roughness plus dielectric perturbations as compared to roughness scattering alone. This can be important when comparing theory and experiment in cases where dielectric fluctuation scattering is in effect. In addition, the polarization ratio can be dependent on the surface and dielectric perturbations statistics, whereas when roughness alone is considered, the polarization ratio is independent of roughness statistics. When comparing ARS data with a roughness-only scattering theory, erroneous conclusions could be drawn if there is dielectric perturbation scattering in effect. This statement applies if the real part of the cross-correlation function G_{rd} is non-negligible. As mentioned above, the sign of the real part is important; for certain assumptions of cross correlation, the overall scattering intensity can be increased or decreased compared to roughness-only theory. Not only could the rms roughness be misinterpreted, but the shape of the ARS curve could also lead to false conclusions regarding the correlation length. On the other hand, if the cross correlation G_{rd} is primarily imaginary in nature, then the results of this work indicate that the roughness-

only theory will suffice since the dielectric scattering is negligible.

The roughness-only theory predicts all of the p to s ratio ($p \rightarrow p$)/($s \rightarrow s$) (shown in the fourth column of Table I) to be 36.2, but the measured ratios are considerably less than this value. The theory considered in this work predicts that the polarization ratio can vary from mirror sample to mirror sample, or spot to spot on the same mirror. This is consistent with experimental ARS measurements from Ag mirrors where the mirrors are produced in an apparently identical fashion. On the assumption that both roughness and dielectric perturbations are in effect, this study can predict some of the salient features of such measurements. For example, since the measured polarization ratios in Table I are less than 36.2, this indicates that the real part of G_{rd} is negative, or that Δz and $\Delta \epsilon$ fluctuate with opposite sign.

The present work, however, does not predict any cross polarization to occur. Experimentally, cross polarization does occur in varying degrees. The amount of measured cross polarization can vary from sample to sample or from point to point on the same sample, as shown in the last column of Table I. In the context of the present study, one possibility of theoretically predicting cross polarization is to let the $\Delta \epsilon(\vec{\rho})$ perturbation be a tensor. Optical properties of films of germanium having voids, where the effective dielectric constant of the composite medium is a tensor, have been discussed elsewhere.¹⁵ A calculation considering the effect of a tensor dielectric perturbation is currently in progress by the author.

ACKNOWLEDGMENTS

Special thanks are due J. M. Bennett for numerous helpful comments and for a critical reading of the manuscript. The author is also indebted to J. P. Rahn, and to J. J. Yeh for many helpful conversations and constructive comments. Support is gratefully acknowledged by the U.S. Naval Weapons Center Independent Research Funds and the U.S. Defense Advanced Research Projects Agency under ARPA Order No. 3343.

APPENDIX A

The Green's-function matrix satisfies the equation

$$\underline{L} \underline{G}(\vec{r}, \vec{r}') = \underline{I} \delta^3(\vec{r} - \vec{r}'), \quad (\text{A1})$$

where \vec{r} and \vec{r}' are the observation and source-location vectors, respectively. The \underline{L} operator is given in the text by Eq. (29). Letting Eqs. (31) be substituted into Eq. (A1) yields

$$\underline{L} \underline{g}(z, z') = \underline{I} \delta(z - z'), \quad (\text{A2})$$

where \underline{I} is the identity matrix, and

$$\underline{L} = \begin{pmatrix} k_y^2 - (\omega/c)^2 \epsilon - \frac{\partial^2}{\partial z^2} & -k_x k_y & ik_x \frac{\partial}{\partial z} \\ -k_x k_y & k_x^2 - (\omega/c)^2 \epsilon - \frac{\partial^2}{\partial z^2} & ik_y \frac{\partial}{\partial z} \\ ik_x \frac{\partial}{\partial z} & ik_y \frac{\partial}{\partial z} & k_x^2 + k_y^2 - (\omega/c)^2 \epsilon \end{pmatrix}. \quad (\text{A3})$$

The solution to the coupled system of equations given by Eq. (A2) yields

$$g_{xx}^{(1,1)}(z, z') = \frac{iq_1}{2\epsilon_1(\omega/c)^2} (e^{iq_1|z-z'|} + R_p e^{-iq_1(z+z')}), \quad (\text{A4})$$

$$g_{yy}^{(1,1)}(z, z') = \frac{i}{2q_1} (e^{iq_1|z-z'|} + R_s e^{-iq_1(z+z')}), \quad (\text{A5})$$

$$g_{xz}^{(1,1)}(z, z') = \frac{-ik}{2\epsilon_1(\omega/c)^2} [\text{sgn}(z-z') e^{-iq_1|z-z'|} + R_p e^{-iq_1(z+z')}], \quad (\text{A6})$$

$$g_{zx}^{(1,1)}(z, z') = \frac{-ik}{2\epsilon_1(\omega/c)^2} [\text{sgn}(z-z') e^{iq_1|z-z'|} - R_p e^{-iq_1(z+z')}], \quad (\text{A7})$$

$$g_{zz}^{(1,1)}(z, z') = -\frac{\delta(z-z')}{\epsilon_1(\omega/c)^2} + \frac{ik^2}{2\epsilon_1(\omega/c)^2} (e^{iq_1|z-z'|} + R_p e^{-iq_1(z+z')}), \quad (\text{A8})$$

where

$$R_p = \frac{q_2\epsilon_1 - q_1}{q_2\epsilon_1 + q_1} \quad (\text{A9})$$

and

$$R_s = \frac{q_1 - q_2}{q_1 + q_2} \quad (\text{A10})$$

for the case where z and z' are both in medium 1; in other words, when the source and observation points are both in the lower medium. In Eq. (A8), the term proportional to the $\delta(z-z')$ is dropped as it does not contribute to the scattered field. The subscripts of the matrix elements of \underline{g} as given in Eqs. (A4)–(A8) refer to the directions of the field at the observation point z due to a given component of the source vector at z' . For example, the $g_{zx}^{(1,1)}$ matrix element is the x component of the field radiated by a source-vector component in the z direction. Equations (A4)–(A8) are calculated for the special case where $k_x = k$ and $k_y = 0$. For Eqs. (A4)–(A8), the wave vector of the radiated field is $(k, 0, -q_1)$. However, to convert this matrix to correspond to a general scattering direction $(k_x, k_y, -q_1)$, a similarity transformation can be used.¹¹ The superscript (1,1) refers to the observation medium and source-location medium, respectively. For the other solution pertinent to this calculation, we find

$$g_{xx}^{(2,1)}(z, z') = \frac{iq_1 q_2}{(\omega/c)^2 (q_2\epsilon_1 + q_1)} e^{i(q_2 z - q_1 z')}, \quad (\text{A11})$$

$$g_{yy}^{(2,1)}(z, z') = \frac{i}{q_1 + q_2} e^{i(q_2 z - q_1 z')}, \quad (\text{A12})$$

$$g_{xz}^{(2,1)}(z, z') = \frac{-ikq_2}{(\omega/c)^2 (q_2\epsilon_1 + q_1)} e^{i(q_2 z - q_1 z')}, \quad (\text{A13})$$

$$g_{zx}^{(2,1)}(z, z') = \frac{-ikq_1}{(\omega/c)^2 (q_2\epsilon_1 + q_1)} e^{i(q_2 z - q_1 z')}, \quad (\text{A14})$$

$$g_{zz}^{(2,1)}(z, z') = \frac{ik^2}{(\omega/c)^2 (q_2\epsilon_1 + q_1)} e^{i(q_2 z - q_1 z')}, \quad (\text{A15})$$

where the source is in medium 1 and observation in medium 2. For this matrix, the radiative wave vector is $(k, 0, q_2)$, and use of the similarity transformation mentioned above yields a radiative wave vector (k_x, k_y, q_2) .

Equations (A4)–(A8) and (A11)–(A15) have been derived subject to the condition that the tangential components of the electric and magnetic fields produced by the Dirac δ -function source are continuous across the boundary $z=0$. In other words,

$$g_{xx}^{(1,1)}(0, z') = g_{xx}^{(2,1)}(0, z'), \quad (\text{A16})$$

$$g_{xz}^{(1,1)}(0, z') = g_{xz}^{(2,1)}(0, z'), \quad (\text{A17})$$

$$g_{yy}^{(1,1)}(0, z') = g_{yy}^{(2,1)}(0, z'), \quad (\text{A18})$$

$$\epsilon_1 g_{zx}^{(1,1)}(0, z') = g_{zx}^{(2,1)}(0, z'), \quad (\text{A19})$$

$$\epsilon_1 g_{zz}^{(1,1)}(0, z') = g_{zz}^{(2,1)}(0, z'). \quad (\text{A20})$$

Equations (A16)–(A20), along with the continuity conditions on the zeroth-order fields, ensure that the first-order fields, as in Eqs. (41) and (42), are continuous in the same fashion as the zeroth-order fields.

APPENDIX B

To obtain a rough estimate of a reasonable value of ζ_d [see Eq. (23)], and to justify the ζ_d values used in this work (1.02 and 2.55), we proceed as follows. For the permittivity of medium 1, assume that the spatial variation is in the plane parallel to the boundary between media 1 and 2 (there is no z variation). For purposes of this estimate, assume a model dielectric permittivity given by

$$\epsilon(\vec{\rho}) = \epsilon_1 + (\zeta - \epsilon_1) \sum_{i=1}^N H(|\vec{\rho} - \vec{\rho}_i|), \quad (\text{B1})$$

where ϵ_1 is a constant background permittivity of the host medium. The Heaviside step function $H(x)$ is unity for $x \leq R$ and zero for $x > R$, where R is the radius of a dielectric perturbation. All dielectric perturbations are assumed to have the same radius and are nonoverlapping. The summation is over the N sites of dielectric perturbations which are randomly located at $\vec{\rho}_i$. This model further assumes that all dielectric perturbations have the same permittivity ζ . Thus, when $|\vec{\rho} - \vec{\rho}_i|$ ($i=1, N$) is less than R , ϵ becomes ζ . When $|\vec{\rho} - \vec{\rho}_i|$ is greater than R , ϵ becomes ϵ_1 . In other words, this model is a host material of ϵ_1 with randomly distributed nonoverlapping columns of radius R with permittivity ζ .

To calculate ζ_d for this model dielectric function, the average value of ϵ is needed. This is obtained by averaging ϵ over area L^2 in the x - y plane as

$$\langle \epsilon \rangle = \frac{1}{L^2} \int d\phi \rho d\rho \epsilon(\vec{\rho}), \quad (\text{B2})$$

which yields

$$\langle \epsilon \rangle = \epsilon_1 + (\zeta - \epsilon_1) \pi N R^2 / L^2. \quad (\text{B3})$$

To find an estimate for ζ_d , we calculate

$$\zeta_d^2 = \langle [\epsilon(\vec{\rho}) - \langle \epsilon \rangle]^2 \rangle = \frac{1}{L^2} \int d\phi \rho d\rho [\epsilon(\vec{\rho}) - \langle \epsilon \rangle]^2. \quad (\text{B4})$$

This integral is easily evaluated and yields

$$\zeta_d^2 = (\zeta - \epsilon_1)^2 f(1-f), \quad (\text{B5})$$

where

$$f = \pi N R^2 / L^2 \quad (\text{B6})$$

is the fraction of the total area of the dielectric perturbations, $\pi N R^2$, to the total area of the surface L^2 . Values

of ζ_d may be inserted in Eq. (B5), and f may be calculated. There will be two solutions, and the smaller is chosen. As an example, the value of ζ may be chosen to be that of AgS_2 , which yields $\zeta = (8.76, 2.49)$,⁵ and ϵ_1 for Ag at $\lambda = 0.6328 \mu\text{m}$ is taken to be $(-16.4, 0.53)$. Omitting their imaginary parts, this yields $(\zeta - \epsilon_1)^2 = 633.03$. With this it may be shown that $f = 0.00165$ for $\zeta_d = 1.02$ and $f = 0.00257$ for $\zeta_d = 2.55$. These values of f indicate that the fractional coverage of the surface area for the dielectric perturbations is quite small and that this would appear to be a physically reasonable possibility. If, instead of a ζ value based on AgS_2 , a ζ value of unity were chosen to be representative of voids, the f values would be 0.00067 and 0.00096, respectively. Because of these small f values, the ζ_d values chosen in this work are taken to be physically realistic.

¹J. M. Elson, J. P. Rahn, and J. M. Bennett, *Appl. Opt.* **19**, 669 (1980).

²J. M. Bennett, J. M. Elson and J. P. Rahn, in *Thin Film Technologies*, edited by J. Roland Jacobsson [Proc. SPIE **401**, 234 (1983)]; J. M. Bennett, J. M. Elson, and K. H. Guenther, *J. Opt. Soc. Am.* **73**, 1937A (1983); J. M. Bennett *et al.*, in Proceedings of the Optical Society of America Spring Conference on Applied Optics, Optical Interference Coatings, April 17–19, 1984 (unpublished).

³Yau Jen Wang and William L. Wolfe, *J. Opt. Soc. Am.* **73**, 1596 (1983).

⁴J. M. Bennett and J. H. Dancy, *Appl. Opt.* **20**, 1785 (1981).

⁵D. K. Burge, J. M. Bennett, R. L. Peck, and H. E. Bennett, *Surf. Sci.* **16**, 303 (1969).

⁶One of the early works in this area was D. E. Barrick, *Radar Cross Section Handbook* (Plenum, New York, 1970), Chap. 9.

⁷Other references related to the method used here include E. Kröger and E. Kretschmann, *Z. Phys.* **237**, 1 (1970); J.

Vliieger and D. Bedeaux, *Physica (Utrecht)* **85A**, 389 (1976); V. Celli, A. Marvin, and F. Toigo, *Phys. Rev. B* **11**, 1779 (1975); J. M. Elson, *ibid.* **12**, 2541 (1975).

⁸See the first of Refs. 7.

⁹J. D. Jackson, *Classical Electrodynamics*, 2nd ed. (Wiley, New York, 1975), pp. 17–22.

¹⁰A. A. Maradudin and D. L. Mills, *Phys. Rev. B* **11**, 1392 (1975).

¹¹D. L. Mills, A. A. Maradudin, and E. Burstein, *Ann. of Phys.* **56**, 504 (1970).

¹²J. S. Bendat and A. G. Piersol, *Random Data: Analysis and Measurement Procedures* (Wiley-Interscience, New York, 1971), pp. 28–31.

¹³J. M. Elson and J. M. Bennett, *J. Opt. Soc. Am.* **69**, 31 (1979).

¹⁴D. K. Burge, H. E. Bennett, and E. J. Ashley, *Appl. Opt.* **12**, 42 (1973). This work also considers wavelengths in the visible range.

¹⁵F. L. Galeener, *Phys. Lett.* **27**, 421 (1971); **27**, 1716 (1971).